
Superradiance in an Optical Lattice

Introduction: Cold atoms experiments are powerful platforms to study many-body quantum systems. When the number of particles of a system N is large, analytical or numerical methods usually fail, as the number of parameters diverges. Cold atoms experiments, through a fine preparation of the atomic mixture (temperature, position...), give access to a very flexible system where Hamiltonians can be tuned at will to explore the different dynamics exhibited by the system (for instance adding a magnetic field will change contact interactions through Feshbach's resonance processes). Working with ultracold atoms can thus give access to a better understanding of complex systems, such as neutron star (for example rotating quantum gases in the supersolid phase can help understanding neutron-star glitches [Poli et al., 2023]).

In ultracold atoms experiments, the temperature imposed to the atoms can reach the nano-Kelvin range. The main goal here is to reduce the thermal motion of the atoms to confine them in various traps (magneto-optical traps, optical lattices, tweezers...). Moreover reaching these temperatures gives access to very sensitive dynamics, as the energies involved are close to the ground state energy of the system, and to exotic phases of quantum matter, such as Bose-Einstein condensates.

At the University of Innsbruck (Austria), the Erbium team traps Erbium atoms in optical lattices (2 counter-propagating lasers creating a standing wave in which atoms are periodically trapped), and characterises the dynamics resulting from their interactions. Erbium has a great manifold of energy levels, but we can experimentally isolate two of these energy levels (an excited state (ES) and a ground state (GS)) to reduce the complexity of the problem to a N body problem of interacting 2-level atoms. The main focus of the team during my stay in Innsbruck was the study of Superradiance (SR), which is a collective effect resulting in an enhanced decay rate of an initially excited system. This enhanced collective decay rate is caused by the electric dipole-dipole interaction, which creates collective decay mechanisms (through stimulated emission in-between the atoms). SR was already experimentally demonstrated in several cold atoms experiments [Inouye et al., 1999], but was never observed in optical lattices.

Furthermore, Erbium atoms also interact via the magnetic dipole-dipole interaction, which effects are of the same order of magnitude as the electric interaction in our experimental situation. As the consequences of magnetic interactions in the dynamics of our system were not completely understood, the main focus of my internship was the simulation of these two interactions at an intermediate scale (a maximum of 75 interacting atoms was achieved). We showed that the magnetic dipole-dipole interaction decreases the SR effect. Additionally, several experimental parameters were added to the model (excitation of the system, filling fraction of the lattice, detuning of the harmonic trap...), in order to simulate a system as close to the experimental one as possible. Experimental side projects (camera support, implementation of an electro optic modulator EOM, and digital PID) were also conducted during the internship, and are presented in the appendix 3.4.

In the first part of this report, the theory of the simulation of open quantum systems and the Superradiant effect will be presented. In the second part, the magnetic dipole-dipole interaction will be added to the system. Finally in the third part, experimental specifics will be added to the model.

Key words : Cold atoms, superradiance, meanfield plus correlation simulations.
Internship monitored by :

Arfor Houwman, Francesca Ferlaino

UIBK

Innsbruck

Special thanks

I would like to especially thank Arfor for this internship. He was an excellent supervisor, full of patience regarding the experimental mistakes I could make over and over again, and very helpful when I was struggling with the simulations. We also shared great moments outside of the lab, with him and the rest of the team, enjoying the city or going to the mountains. For all of these moments, I will remember my time in Innsbruck as a very fulfilling and fun internship.

Many thanks to Louis and Sarah for their precious advices and the great discussions we had about physics or any other subject, and also for the amazing dinners and cake you both prepared, it was delicious! It was a real pleasure working with both of you.

Finally, I would like to thank Francesca Ferlaino and the rest of the team who welcomed me to Innsbruck. The social events we had were really cool (and delicious again), the talks of the different students or professors who visited the lab were really interesting, and the general conditions of work and mutual assistance of this laboratory were particularly enjoyable.

Many thanks to all of you!

Contents

1 Theory of Superradiance and electric dipole-dipole interaction	1
1.1 Lindblad master equation	1
1.1.1 Experimental situation	3
1.2 Electric dipole-dipole interaction	4
1.3 First simulations, effect of the electric dipole-dipole interactions	5
1.3.1 Mean-field	5
1.3.2 Mean-field plus correlations	6
1.3.3 Solving the system	6
1.4 First results: Choice of the laser	6
1.5 SR criterium	7
2 Adding the magnetic dipole-dipole interaction	7
2.1 Theoretical description of the magnetic dipole-dipole interaction	7
2.2 Symbolic computation of the MPC equations	9
2.3 Effect of the MDDI on SR	10
3 Exploring the experimental parameters	12
3.1 Coherent <i>versus</i> incoherent excitations	12
3.2 Initial number of ES	15
3.3 Filling fraction	15
3.4 Harmonic trap detuning	16

1 Theory of Superradiance and electric dipole-dipole interaction

A table of all the symbols and their significations can be found in [3.4](#).

1.1 Lindblad master equation

In the theory of open quantum systems, the Lindblad master equation (ME) plays a key role, as the most general generator of Markovian dynamics (memoryless dynamics) [[Manzano, 2020](#)].

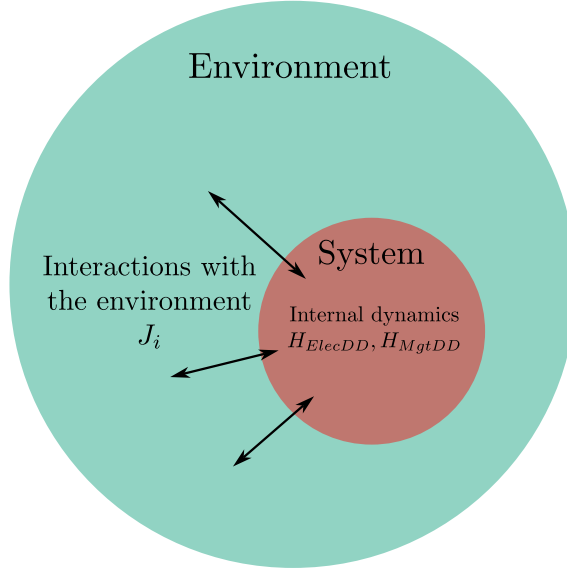


Figure 1: Scheme of our open quantum system: The system has internal dynamics (atoms in the optical lattice interact *via* the electric (H_{ElecDD} + collective decay $\Gamma_{i \neq j}$ matrix) and magnetic (H_{MgtDD}) dipole-dipole interaction (see section [1.2](#) and [2](#)). It also exchanges energy with the environment via the emission of photons lost in the environment (jump operators J_i).

It can be written as:

$$\partial_t \rho = -\frac{i}{\hbar} [H, \rho] + \mathcal{L}[\rho] \quad (1)$$

with $\mathcal{L}[\rho]$ the Lindblad superoperator:

$$\mathcal{L}[\rho] = \sum_{i,j} \Gamma_{i,j} (J_i \rho J_j^\dagger - \frac{1}{2} \{ J_i^\dagger J_j, \rho \}) \quad (2)$$

where H is the Hamiltonian of the system, $\Omega_{i,j}$ and $\Gamma_{i,j}$ are respectively the interaction and decay matrices and J_i are the jump operators (losses of the system to the environment). The sum runs over all the atoms of our system.

Our system is open, as atoms loose their energy through decay processes, which create photons that can be lost in the environment. This mechanism is taken into account thanks to the Lindblad superoperator. Furthermore, the internal dynamics of our system, such as atoms interacting with each other, can be defined with the appropriate Hamiltonian H . To get this form of the ME, the Born-Markov approximation was made, which is valid for our system (see appendix [3.4](#)).

The matrix $\Gamma_{i,j}$ coefficients are linked to the single and collective decay rates: the i -th on-diagonal term $\Gamma_{i,i}$ corresponds to spontaneous emission (SE) of the i -th atom while the off-diagonal terms $\Gamma_{i \neq j}$ correspond to the collective decay of two different atoms.

Let's further describe these two different decay processes:

- SE: For a single initially excited atom, we can write the probability to find the state in the ES after a time t as: $\mathcal{P}_{ES}(t) = e^{-\gamma t}$, with γ the SE decay rate. For N non-interacting atoms, we can thus write the population of the ES as : $\mathcal{P}_{ES}(t) = N_{ES}(t_0)e^{-\gamma t}$ where $N_{ES}(t_0)$ is the initial number of atoms in the excited state ($N_{ES}(t_0) \leq N$).
- Collective decay: This decay process happens for interacting atoms, and leads to the phenomenon of Superradiance (SR). SR is a collective mechanism that leads to a faster relaxation of the system compared to SE. It was originally suggested by R. H. Dicke in 1953 [Dicke, 1954]. To illustrate SR, let's start with a simple example of the Dicke model taken from [Gross and Haroche, 1982], where the decay rate of the system is fully derived. We consider N indistinguishable 2-level atoms initially in the ES, only interacting with a radiation field. The atoms are assumed to be point particles located at the same position. We can write the state of the system as $|J, M\rangle$ where $J = N/2$, and $J + M$ is the number of atoms in the ES, $J - M$ atoms being in the GS.

$$|J, M\rangle = \mathcal{S} \underbrace{|\uparrow\uparrow\dots\uparrow\uparrow\rangle}_{J+M} \underbrace{|\downarrow\downarrow\dots\downarrow\downarrow\rangle}_{J-M} \quad (3)$$

where \mathcal{S} is the symmetrisation operator. We make the assumption that the coupling of the atoms to the radiation field is symmetrical with respect to the exchange of any two atoms in the system¹. The decay rate of the system can then be written as: $\mathcal{W}(t) = \partial_t \mathcal{P}_{ES}(t) = \Delta\nu_0 \langle \sigma^+ \sigma^- \rangle$ where $\Delta\nu_0$ is the atomic natural linewidth of a single atom², and $\sigma^{+/-} = \sum_i \sigma_i^{+/-}$ are the collective ladder operators. From the properties of the ket $|J, M\rangle$, we can compute $\mathcal{W}^{J,M}$ which is the decay rate of the state $|J, M\rangle$:

$$\mathcal{W}^{J,M} = \langle J, M | \mathcal{W} | J, M \rangle = \Delta\nu_0 (J + M)(J - M + 1) \quad (4)$$

$\mathcal{W}^{J,M}$ is plotted on figure 2 with respect to the quantum number M for a system of 21 atoms. At the beginning of the decay of the system, $\mathcal{W}^{J,M}$ increases until it reaches its maximum for $M = 0$, where the system is semi-inverted (half of the atoms are in the ES, the other half is in the GS). It then decreases and reaches 0 for $M = -J$ (all the atoms are then in the GS).

SR is deeply connected to the correlations between the atoms. Indeed, these correlations can be written for our system as:

$$\langle J, M | \sigma_i^+ \sigma_j^- | J, M \rangle = \frac{J^2 - M^2}{N(N-1)} \quad (5)$$

Correlations also reach their maximum for $M = 0$. The system will thus act as a global radiating dipole of magnitude proportional to N , and the photon emission (or the decay rate) will thus be proportional to N^2 .

In our system, we can also give a semi-classical picture of SR: the decay of the i -th atom creates a (virtual) photon that can cause the stimulated emission of the j -th atom. The resulting collective decay rate is encapsulated in the term $\Gamma_{i \neq j}$, the two atoms being correlated. This mechanism can cause a cascade of stimulated emissions which will relax the system much faster than the independent case, and emit a sudden burst of photons.

We can finally add that in real systems, the coherent light emission of a SR decay is not trivial, and strongly depends on the excitation and the geometry of the system [Inouye et al., 1999].

To have a mathematical illustration, let's write the Lindblad superoperator $\mathcal{L}[\rho]$ for 2 identical interacting atoms with the same SE decay rate γ . $\mathcal{L}[\rho]$ will be the sum of 4 terms, as i and j run over the 2 atoms, and the jump operator will be the ladder operators $J_i = \sigma_i^+$ and $J_i^\dagger = \sigma_i^-$. We can thus

¹This hypothesis is more precisely discussed in [Gross and Haroche, 1982], as it isn't necessarily true even for atoms confined in a small volume compared to the radiation field wavelength.

²This is a generalisation of the rate of photon emission for a single atom, which can be written as $\mathcal{W}_i(t) = \Delta\nu_0 \langle \sigma_i^+ \sigma_i^- \rangle$.

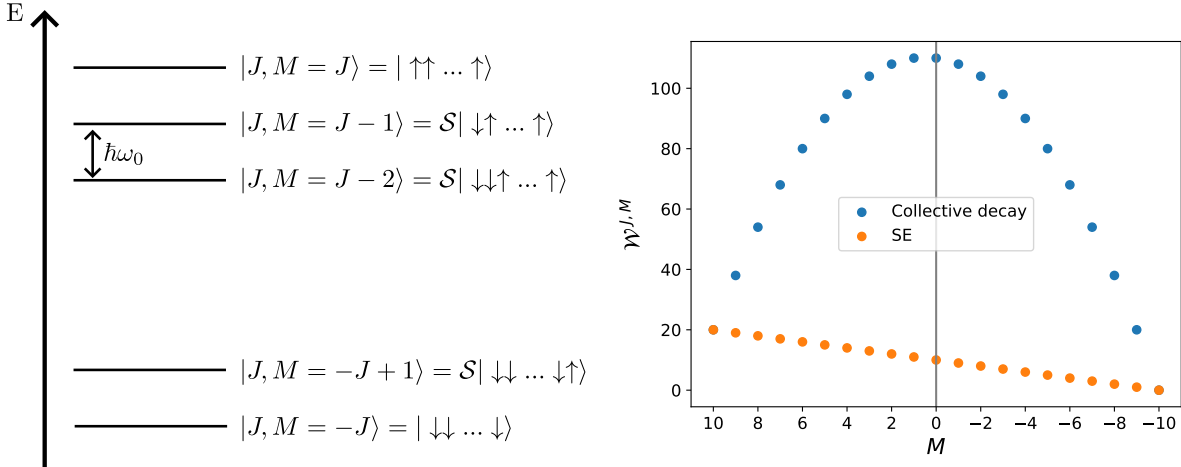


Figure 2: Left: Dicke ladder. The different $|J, M\rangle$ states are separated by the energy $\hbar\omega_0$, which is the energy difference between the ES and the GS for a single atom. Right: Decay rate $\mathcal{W}^{J,M}$ as a function of M . In orange, the atoms are independent and decay because of SE only. In blue, collective decay is taken into account. The maximum of $\mathcal{W}^{J,M}$ is reached for $M = 0$ (and $M = 1$, which has the same decay rate).

write the decay matrix as: $\Gamma = \begin{pmatrix} \gamma & \Gamma_{1,2} \\ \Gamma_{2,1} & \gamma \end{pmatrix}$. By symmetry of the problem, $\Gamma_{1,2} = \Gamma_{2,1}^*$. As the Γ matrix is real (see section 1.2), we can diagonalize Γ to $D = \begin{pmatrix} \gamma + \Gamma_{1,2} & 0 \\ 0 & \gamma - \Gamma_{2,1} \end{pmatrix}$ with $\Gamma = PDP^{-1}$ and $P = P^{-1} = \frac{1}{\sqrt{2}} \begin{pmatrix} 1 & 1 \\ 1 & -1 \end{pmatrix}$.

The Lindblad term then becomes:

$$\mathcal{L}[\rho] = \sum_a D_{a,a} (L_a \rho L_a^\dagger - \frac{1}{2} \{L_a^\dagger L_a, \rho\}) \quad (6)$$

with $L_a = \sum_i P_{i,a} J_i = \sum_i P_{i,a} \sigma_i^+$. Thus, $L_1 = \frac{1}{\sqrt{2}}(\sigma_1^+ + \sigma_2^+)$ and $L_2 = \frac{1}{\sqrt{2}}(\sigma_1^+ - \sigma_2^+)$, which are collective jump operators.

Thanks to this diagonalization, we can see that the system will decay with two different rates, and with the collective jump operators L_a instead of J_i . The first decay rate, associated to L_1 , gives a faster decay of the system than SE and leads to SR. The second, associated to L_2 , is smaller than γ and leads to Subradiance³. From the form of the collective jump operators L_a , we can say that SR is the in-phase collective decay and Subradiance is the out-of-phase collective decay of two atoms.

From this simple example it is clear that Super- and Subradiance effects come hand in hand when solving collective decay, as we will see in section 1.4.

1.1.1 Experimental situation

Our experimental situation is the following: A maximum of 10^4 ^{166}Er atoms are trapped in a tetragonal optical lattice. Erbium atoms have a huge manifold of energy levels, but we can experimentally isolate two of them, reducing the problem to a 2-level problem of N interacting atoms. The ES is $|J = 7, m_J = -7\rangle$ and the GS is $|J = 6, m_J = -6\rangle$ where J is the total angular momentum and m_J its projection along the quantization axis [Claude et al., 2024]. Thus, if we start from a fully-inverted system, the initial expectation value of the spin along the z-axis, averaged over all the atoms, will be $\langle \sigma_z \rangle = -7$. During the decay of the system, $\langle \sigma_z \rangle$ will increase until it reaches -6 when all the atoms

³Subradiance is the opposite effect of SR: collective effects leading to a decreased decay rate of the system compared to the independent case [Rui et al., 2020].

are in the GS. $\langle \sigma_z \rangle$ is thus directly proportional to the population in the ES and in the GS, and we will use in the following this expectation value to track the decay of the system.

The distance between each lattice site is 266 nm for the horizontal plane, and 532 nm for the vertical plane (see figure 3). Atoms are close enough to effectively interact with each other *via* the electric and magnetic dipole-dipole interaction (EDDI and MDDI respectively), which will be described in the next sections. EDDI will mean that we took into account H_{ElecDD} and the collective decay matrix Γ , while MDDI will mean that H_{MgtDD} was incorporated to the simulations. We will then explore the dynamics produced by these two kinds of interactions.

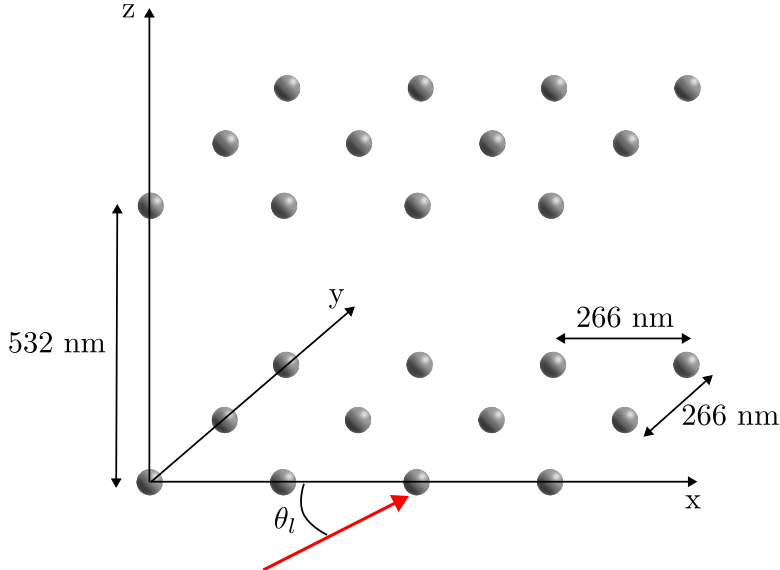


Figure 3: A scheme of the optical lattice: 10^4 Erbium atoms are trapped in a tetragonal optical lattice of dimensions $266 \times 266 \times 532$ nm. The red arrow is the direction of the excitation laser (which is in the horizontal plane). The angle it makes with the x-axis will be named θ_l (see section 3.1).

1.2 Electric dipole-dipole interaction

Erbium atoms do not have an electric dipole moment in the GS or ES. However, we can associate to the transition $|\downarrow\rangle \rightarrow |\uparrow\rangle$ an electric dipole moment [Baßler et al., 2024]:

$$\vec{d}_{\uparrow\downarrow} = -\langle \uparrow | e\mathbf{r} | \downarrow \rangle = -e \int_{\mathbb{R}} \psi_{\uparrow}(\vec{r}) \vec{r} \psi_{\downarrow}(\vec{r}) d\vec{r} \quad (7)$$

where \mathbf{r} is the position operator and e the elementary charge.

If we excite an atom with a resonant electromagnetic field, the atom can either absorb or emit (via stimulated emission) photons. We can write this mechanism as an electric dipole operator acting on the atom:

$$\mathbf{d} = \vec{d}_{\uparrow\downarrow} \sigma^+ + \vec{d}_{\uparrow\downarrow}^* \sigma^- \quad (8)$$

where σ^{\pm} are the ladder operators. For a single atom, this electric dipole operator leads to Rabi oscillations: Under continuous excitation by a resonant light, an atom will oscillate between the GS and the ES (see appendix 3.4).

Moreover, the atoms of Erbium are close enough (see section 1.5) in the lattice to interact effectively *via* the electric dipole-dipole interaction with each other.

The effect of the electric dipole-dipole interactions can be taken into account in the ME 1 by:

- A collective Hamiltonian that results in a spin-flip exchange between two different atoms:

$$H_{\text{ElecDD}} = \sum_{i \neq j} \Omega_{i,j} \sigma_i^+ \sigma_j^- \quad (9)$$

where $\Omega_{i,j} = \frac{3}{4}\gamma G(k_0 r_{i,j})$.

- Off-diagonal terms in the decay matrix: $\Gamma_{i,j} = \frac{3}{2}\gamma F(k_0 r_{i,j})$ that will create collective decay dynamics such as SR.

The functions F, G come from the Green's function solution for an electric dipole radiating into free space, and are given by [Bettles et al., 2016], [Jackson, 2021]:

$$F(\xi) = \alpha \frac{\sin \xi}{\xi} + \beta \left(\frac{\cos \xi}{\xi^2} - \frac{\sin \xi}{\xi^3} \right) \quad (10)$$

$$G(\xi) = -\alpha \frac{\cos \xi}{\xi} + \beta \left(\frac{\sin \xi}{\xi^2} + \frac{\cos \xi}{\xi^3} \right) \quad (11)$$

where $\alpha = 1 - \cos^2 \theta$ and $\beta = 1 - 3 \cos^2 \theta$, with θ the angle between the vector $r_{i,j}$ connecting atoms i and j and $d_{\uparrow\downarrow}$. This approach is semi-classical: the atoms are treated quantum mechanically, while the matrix of the spin-flip exchange Hamiltonian Ω and the decay matrix Γ are computed in a classical framework.

We will show in the following that in our experimental situation the electric dipole-dipole interaction causes SR, while the magnetic interaction reduces its effect.

1.3 First simulations, effect of the electric dipole-dipole interactions

All the simulations can be accessed at the following Github <https://github.com/DolbeaultRemy/M2Internship.git>.

In this subsection, we will present simple simulations showing the SR effect, with EDDI only. These first results will also help us choosing the best experimental parameters to observe SR. The magnetic interaction will be added in section 2.

The *CollectiveSpins.jl*⁴ library is an implemented package for the *Julia* language that allows an easy computation of the dynamics of N 2-level atoms placed on a lattice, interacting only via the EDDI.

As all the operators and the density matrix sizes scale as 2^N , the ME can only be solved for a small number of atoms (see 3.4). In order to compute the dynamics of the system for a bigger number of atoms and clearly simulate collective effects, mean-field (MF) or mean-field plus correlations (MPC) computations can be done with this library. Let's take $a, b, c \in \{x, y, z\}$ and $i, j, k \in \llbracket 1, N \rrbracket$.

1.3.1 Mean-field

The MF equations of the expectation values of $\langle \sigma_i^a \rangle$ can be computed starting from the ME and applying the commutation rules of the Pauli matrices. Indeed:

$$\partial_t \langle \sigma_i^a \rangle = \partial_t \text{Tr}(\sigma_i^a \rho) = \text{Tr}(\sigma_i^a \partial_t \rho) \quad (12)$$

By replacing $\partial_t \rho$ with the ME 1, and using the cyclic properties of the trace and the commutation rules of the Pauli operators, we can compute a first-order differential equation for $\langle \sigma_i^a \rangle$. This equation depends on 2-body correlation functions $\langle \sigma_i^a \sigma_j^b \rangle$. For a MF approach, we stop at the first order and replace these 2-body correlation functions with a cumulant expansion method [Kubo, 1962] to close the set of differential equations (see 3.4):

$$\langle \sigma_i^a \sigma_j^b \rangle = \langle \sigma_i^a \rangle \langle \sigma_j^b \rangle \quad (13)$$

⁴No citation was found for this library, so here is a link to the documentation website of this package: <https://qojulia.github.io/CollectiveSpins.jl/>.

1.3.2 Mean-field plus correlations

To go beyond MF and take into account 2-body correlations between the atoms, which are necessary to describe the interactions between the atoms (see appendix 18), we use MPC computations: We add to the previous set of equations the differential equations of the 2-body correlation functions $\langle \sigma_i^a \sigma_j^b \rangle$. To close our system of equations, we then approximate the 3-body correlations functions that appear in these new equations with a cumulant expansion of order 3 (see 3.4):

$$\langle \sigma_i^a \sigma_j^b \sigma_k^c \rangle = \langle \sigma_i^a \sigma_j^b \rangle \langle \sigma_k^c \rangle + \langle \sigma_i^a \sigma_k^c \rangle \langle \sigma_j^b \rangle + \langle \sigma_i^a \rangle \langle \sigma_j^b \sigma_k^c \rangle - 2 \langle \sigma_i^a \rangle \langle \sigma_j^b \rangle \langle \sigma_k^c \rangle \quad (14)$$

With MPC computations, we can then easily compute system with a typical size of $5 \times 5 \times 3 = 75$ atoms, which will be enough as discussed in 1.4 to simulate the collective behaviour of our system. A comparison of MPC simulations and full solution of the ME, as well as the dependency of the dynamics with respect to the lattice dimensions can be found in appendix 3.4.

1.3.3 Solving the system

The obtained set of differential equations is then solved using the *DifferentialEquations.jl* library [Rackauckas and Nie, 2017]. This package optimises the integration of a set of differential equations by using adaptive time steps and offers a wide choice of solvers. The *CollectiveSpins.jl* library uses the Dormand-Prince's method (see 3.4).

1.4 First results: Choice of the laser

Four lasers with different wavelengths ($\lambda = [583, 631, 841, 1299]\text{nm}$) are used in the experiment. Each one is resonant with a transition of Erbium, so SR should be observable with everyone of them. However, as the distance between the atoms is fixed by the lattice beams, some of these lasers will be more efficient than others in enhancing SR.

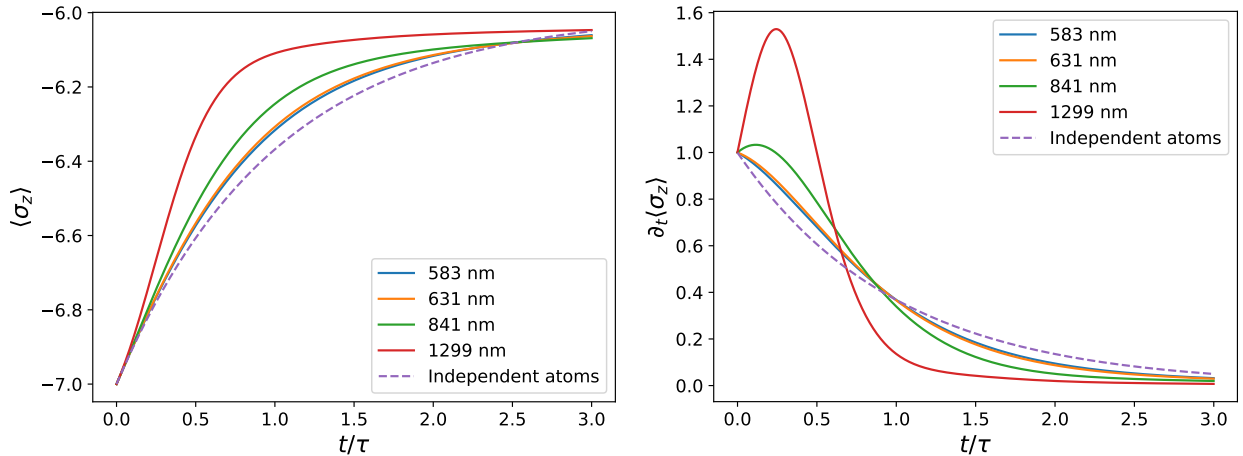


Figure 4: Mean value of $\langle \sigma_z \rangle$ (left) and it's time derivative (right) as a function of the normalised time ($\tau = 1/\gamma$) for the different lasers used in the experiment, starting from a fully inverted system, using MPC computations from the *CollectiveSpins.jl* library. There is $5 \times 5 \times 3 = 75$ atoms in a lattice with our experimental dimensions ($266 \times 266 \times 523\text{ nm}$). The SR burst increases for higher values of λ , as more atoms are effectively interacting for bigger wavelengths. This burst roughly scales as N_λ^2 , with N_λ the number of atoms in a volume λ^3 .

Indeed, in the left plot of figure 4, we can see for all the different lasers that atoms decay faster than the independent case, where only SE plays a role (dashed line). In the right figure, we plotted the derivative of $\langle \sigma_z \rangle$, which is directly proportional to the number of emitted photons. This derivative

shows a burst: At initial times, a few atoms decay and correlations are built in our system, until the maximum emission rate is achieved (at $t/\tau \approx 0.3$ for $\lambda = 1299$ nm). After this burst, the decay rate quickly drops down, and becomes smaller than the independent case in order to ensure energy conservation. This effect is called the Subradiant tail. Indeed, as the interacting system released energy faster than the independent case at the beginning of the dynamics, it has to decay slower after a certain amount of time to ensure that when $t \rightarrow +\infty$, the same amount of energy was released in both cases.

We can see on figure 4 that the bigger the wavelength of the laser is, the more pronounced the SR effect. Indeed, the EDDI is proportional to terms of order up to $O(1/\xi^3)$ when $\xi \rightarrow 0$ (see section 1.2), where $\xi = k_0 r_{i,j}$ with $r_{i,j}$ the distance between two atoms and k_0 the wave-number of the laser. At first order, we can thus assume that the EDDI is not negligible only for couple of atoms $\{i, j\}$ with $r_{i,j} \leq \lambda$. As SR effect is more pronounced if more atoms are involved, the $\lambda = 1299$ nm is the better laser to use in our experiment. In the following, we will use this λ for our simulations.

Moreover, we can approximate the number of atoms that we need to simulate to encapsulate collective effects. In the horizontal plane, the spacing between two atoms is 266 nm, which is 5 times smaller than the wavelength $\lambda = 1299$ nm. Thus atoms interact with approximately 5 neighbours atoms in each direction, for a total of 25 atoms per plane. In the vertical direction, the inter-atom spacing is twice bigger (523 nm), so the atoms can effectively interact with at most 3 neighbours. Thus, if we simulate $5 \times 5 \times 3 = 75$ atoms, we should correctly get the dynamics of the atoms in the centre of the lattice. This approximation is however limited, as geometric resonances appear because of the $1/\xi$ terms in the EDDI (see equations 10 and the next section 1.5), but the effect of these resonances is small compared to the other terms, and can therefore be neglected.

Finally, in some situations were a lot of simulations were needed (see section 3.2 for instance), we used a $5 \times 5 \times 1$ lattice to make the computations faster. This approximation can be justified by the fact that as the inter-atomic distance along the vertical axis is twice the one in the horizontal plane, the interactions between atoms located on top of each other can be at a first order neglected, making the different planes of the lattice independent from each other.

1.5 SR criterium

In order to characterise SR, we need a criterium telling us how strong SR is without having to look at the entire dynamics. Several criteria can be suggested:

The most simple one is the initial value of the time derivative of $\langle \sigma^z \rangle$, normalised by the one of the independent case:

$$\mathcal{C} = \frac{\partial_t \langle \sigma^z \rangle}{\partial_t \langle \sigma_{idp}^z \rangle}(t=0) \quad (15)$$

If $\mathcal{C} > 1$, then we will have a SR effect, followed by a subradiant tail.

Other criteria, such as the maximum decay rate, or the variance of the eigenvalues of the Γ matrix can be used [Masson et al., 2024]. These others criteria give similar results for the EDDI. When the magnetic dipole-dipole interaction (MDDI) is added, some of these criterions can distinguish between EDDI and EDDI + MDDI, and others cannot, as discussed in section 3.3.

We can see on figure 5 geometric resonances: \mathcal{C} can have sudden revivals for some values of the horizontal spacing (for instance for $d_H/\lambda \approx 0.6$). These resonances are linked to the $1/\xi$ term in the Green functions 10 and 11 [Bettles et al., 2016], which will create these long distance SR effects.

2 Adding the magnetic dipole-dipole interaction

2.1 Theoretical description of the magnetic dipole-dipole interaction

Erbium atoms also exhibit a transition magnetic moment, but its effect is negligible. Indeed, let's recall the transition electric dipole moment (see section 1.2):

$$\vec{d}_{\uparrow\downarrow} = -\langle \uparrow | e\mathbf{r} | \downarrow \rangle \quad (16)$$

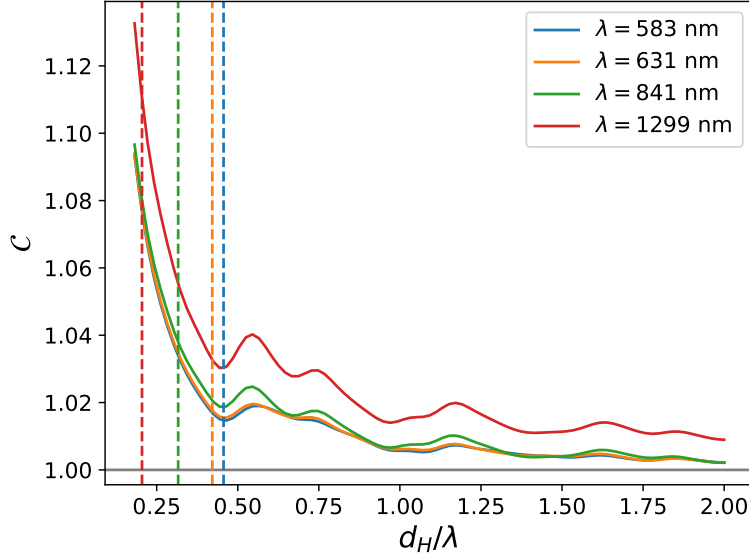


Figure 5: Criterium for SR for each laser as a function of the distance between the atoms in the horizontal plane normalised by λ for a $5 \times 5 \times 3 = 75$ lattice (the vertical distance is fixed at $d_z = 532$ nm), for an initially fully-inverted system. If $C \geq 1$, than the atoms initially decay faster than independent atoms. The dotted vertical lines correspond to the experimental lattice distances for each laser. We can see geometric resonances near $d_H/\lambda \approx 0.6$. For $d_H \gg \lambda$, we recover the independent case, as the interactions can be neglected for inter-atomic distances $r_{i,j} \gg \lambda$.

Similarly, the transition magnetic dipole moment can be written as:

$$\vec{\mu}_{\uparrow\downarrow} = -g_J\mu_B \langle \uparrow | \mathbf{J} | \downarrow \rangle \quad (17)$$

where \mathbf{J} is the angular momentum operator. Since the transition magnetic dipole is negligible compared to the electric one ($e/g_J\mu_B \approx 10^4$), we can in the following neglect it.

However, the static magnetic moment of Erbium atoms in our GS and ES is one of the highest of the periodic table. This magnetic moment is not a transition dipole moment, but an intrinsic magnetic moment of spin that atoms exhibit regardless of the transition. For instance, $\mu_\downarrow \approx g_J\mu_B\sqrt{J(J+1)} \approx -7\mu_B$ for our GS [Smith and Spalding, 1961] [Natale, 2017], where μ_B is the Bohr magneton and g_J the Landé factor. This exceptional value of μ makes the magnetic dipole-dipole interaction (MDDI) effects comparable to the EDDI [Chomaz et al., 2022].

We can write the static magnetic moments of Erbium atoms in the GS and ES as:

$$\vec{\mu}_\uparrow = -g_J\mu_B \langle \uparrow | \mathbf{J} | \uparrow \rangle \quad (18)$$

and

$$\vec{\mu}_\downarrow = -g_J\mu_B \langle \downarrow | \mathbf{J} | \downarrow \rangle \quad (19)$$

The dipole-dipole interaction potential for two magnetic dipoles is:

$$V_{dd}(r_{i,j}) = \frac{\mu_0}{4\pi r_{i,j}^3} \left(\vec{\mu}_i \cdot \vec{\mu}_j - \frac{3(\vec{\mu}_i \cdot \vec{r}_{i,j})(\vec{\mu}_j \cdot \vec{r}_{i,j})}{r_{i,j}^2} \right) \quad (20)$$

where $\vec{\mu}_i = \vec{\mu}_{\uparrow,i} + \vec{\mu}_{\downarrow,i}$. Expanding $V_{dd}(r_{i,j})$ into σ_z and ladder operators $\sigma^{+/-}$, we get the following Hamiltonian [Gorshkov et al., 2011]:

$$H_{\text{MgtDD}} = \sum_{\langle i,j \rangle} \frac{1}{r_{i,j}^3} \left(\frac{J_z}{2} \sigma_i^z \sigma_j^z + \frac{J_\perp}{2} \sigma_i^+ \sigma_j^- \right) \quad (21)$$

Where J_{\perp} and J_z are exchange coupling constants, and the sum runs over nearest neighbours. However, as our two states are of the form $|J, m_J = -J\rangle$, the term J_{\perp} , which is proportional to $\sqrt{J(J+1) - m_J(m_J-1)}$, is null. Thus, we can simplify H_{MgtDD} to:

$$H_{MgtDD} = \sum_{\langle i,j \rangle} \Omega_{i,j}^{mgt} \sigma_i^z \sigma_j^z \quad (22)$$

However, we cannot apply directly this Hamiltonian in our simulations. Indeed, we simulate Spin(1/2) atoms, and after the computations we map the values of the spin from $[-1/2, +1/2]$ to $[-6, -7]$. For the EDDI, taking Spin(1/2) atoms instead of our real 2-level system doesn't change anything, as only ladder operators are involved, which are general for any 2-level system. However for the MDDI, some care is needed, as the sign of the product of the spins can be either positive or negative in a Spin(1/2) system, while in our system it can only be positive (see 3.4 for an illustration of this issue). The solution implemented was to rewrite H_{MgtDD} with the population operators n_i^{\uparrow} and n_i^{\downarrow} which are respectively the population operator of atom i in the ES/GS.

We can then rewrite the Hamiltonian as:

$$H_{MgtDD} = \sum_{\langle i,j \rangle} (a n_{ij}^{\uparrow\uparrow} + b(n_{ij}^{\uparrow\downarrow} + n_{ij}^{\downarrow\uparrow}) + c n_{ij}^{\downarrow\downarrow}) \quad (23)$$

where $n_{ij} = n_i n_j$. The coefficients $[a, b, c]$ are then calculated from equation 20. For instance, the coefficient a is:

$$a = \frac{\mu_0}{4\pi r^3} (\vec{\mu}_{\uparrow} \cdot \vec{\mu}_{\uparrow} - \frac{3(\vec{\mu}_{\uparrow} \cdot \vec{r})(\vec{\mu}_{\uparrow} \cdot \vec{r})}{r^2}) \quad (24)$$

where r is the distance between nearest neighbours and μ_0 is the magnetic constant.

As the inter-atomic distance along the vertical axis is twice the distance in the horizontal plane, and H_{MgtDD} scales as $1/r_{i,j}^3$, we can neglect the MDDI for two neighbouring atoms along the vertical axis, and set $r = 266$ nm for the computation of the $[a, b, c]$ frequencies. We then get $[a, b, c] = [53, 42, 33]$ Hz. The vectors $\vec{\mu}$ are oriented along the quantisation axis, which is set by the applied external magnetic field. In the following, this quantisation axis will be taken along the vertical axis.

2.2 Symbolic computation of the MPC equations

The *CollectiveSpins.jl* library is only implemented for atoms interacting via the EDDI. However, as we would like to simulate the full dynamics of Erbium atoms, we also need to take into account the MDDI. To do so, several techniques have been attempted:

- Full computation of the Lindblad master equation: We compute the EDDI decay matrix Γ and Ω matrix using the *CollectiveSpins.jl* library. We then construct H_{ElecDD} and H_{MgtDD} , and the initial state of the system, and finally solve the ME thanks to the *QuantumOptics.jl* library. This method returns the full density matrix $\rho(t)$, and only needs the assumptions used to derive the ME (see appendix 3.4). However, as discussed in section 1.3, the number of atoms it can simulate must remain small (typically 8 atoms), or the computation time and memory needed will diverge (see 3.4). This method was still used to benchmark the MPC simulations (see 3.4).
- Analytical derivation of the MPC equations: By calculating by hand the temporal derivatives of the expectation values and the 2-body correlation functions, we can write the complete set of MPC differential equations, and solve them using *DifferentialEquations.jl*. However the calculations quickly become cumbersome and prone to error. Moreover, if we want to add a new Hamiltonian (see section 3.4), they need to be recalculated again.
- Symbolic derivation of the MPC equations: The library *QuantumCumulants.jl* [Plankensteiner et al., 2022] symbolically calculates the closed set of differential equations needed to do MPC simulations of the expectation values of the Pauli operators, in the frame of the Lindblad ME 1. This method is very versatile, as Hamiltonians can be added at will without too much effort.

Moreover, the order of the cumulant expansion can be set at any order⁵ if the second order (MPC) is not accurate enough (in our case, order 2 was sufficient as shown in section 3.4).

Many-body Hilbert spaces and transition operators with their commutation relationships are first defined. From these objects, the Hamiltonian of our system can be symbolically reconstructed. At this step, the sums of our two Hamiltonian (EDDI + MDDI) run over a symbolic number of atoms. This library then calculates the set of differential equations of the expectation values of the Pauli operators to a given order n , replacing higher terms with the cumulant expansion method of order n (see 3.4), and simplifying the expressions with the commutation relationships. It then automatically closes the system of differential equation by adding the lacking differential equations. At this stage, we have a set of closed symbolic differential equations, that are valid for any number of atoms N .

We then evaluate the sums, replacing the symbolic number of atoms by the wanted one. The parameters of the system, such as the collective decay Γ and Ω matrices for the EDDI, or the values of the $[a, b, c]$ frequencies for the MDDI, are then inserted. At this point, we get a set of differential equations (up to 14000 for 75 atoms!) with developed sums and numeric values for the parameters.

We then transform these equations to C code functions for two main reasons:

- Parallel compilation of the built functions: In *Julia*, the functions are pre-compiled, meaning that when a function is used for the first time, it is first pre-compiled to an efficient native code form so that the next calls will be much more efficient. However, this compilation can take a very long time for this amount of functions. Using C functions, this compilation can be done in parallel, which makes this step much faster on a multi-core computer.
- In *Julia*, the pre-compiled functions are not saved, so the pre-compilation step has to be done at every new *Julia* session (except if the entire session was saved, but this is not trivial and can cost a lot of memory and time). On the other hand, once the C functions have been compiled, they can be saved in their compiled form and directly called from *Julia*.

Finally, the C functions are called from another *Julia* script, and solved using the same solver as the one of the *CollectiveSpins.jl* library (see section 3.4). For a big number of equations, the number of calls of C functions from a *Julia* script has to be constrained, as calling a C function from *Julia* takes time and memory. To solve this issue, we created a C function that handles the calls to all the other functions. We thus have only one call to make from the *Julia* solving script.

In the following, we will present the results of the symbolic derivation of the MPC equations method. A comparison of these simulations versus the full computation of the Lindblad ME for a small number of atoms can be found in the appendix 3.4.

2.3 Effect of the MDDI on SR

On figure 6, we compared the evolution of $\langle \sigma_z \rangle$ for a system of $5 \times 5 \times 3$ atoms with and without the MDDI, for an initially fully-inverted system:

Several things can be noticed on the influence of the MDDI on the evolution of the system:

- Adding the MDDI decreases the SR effect, as the decay of the system is much slower than with the EDDI only.
- For initial time ($t/\tau \leq 0.1$), the dynamics of the system is not influenced by the MDDI (even in the decay rate plot). This can be understood as follows: H_{MgtDD} is a product of σ_i^z operators,

⁵In practice, the number of differential equations that we will have to solve scales as N^n where n is the order of the cumulant expansion method used. Thus the complexity of the problem quickly diverges for orders higher than 2, at least if we want to simulate a relatively big number of atoms.

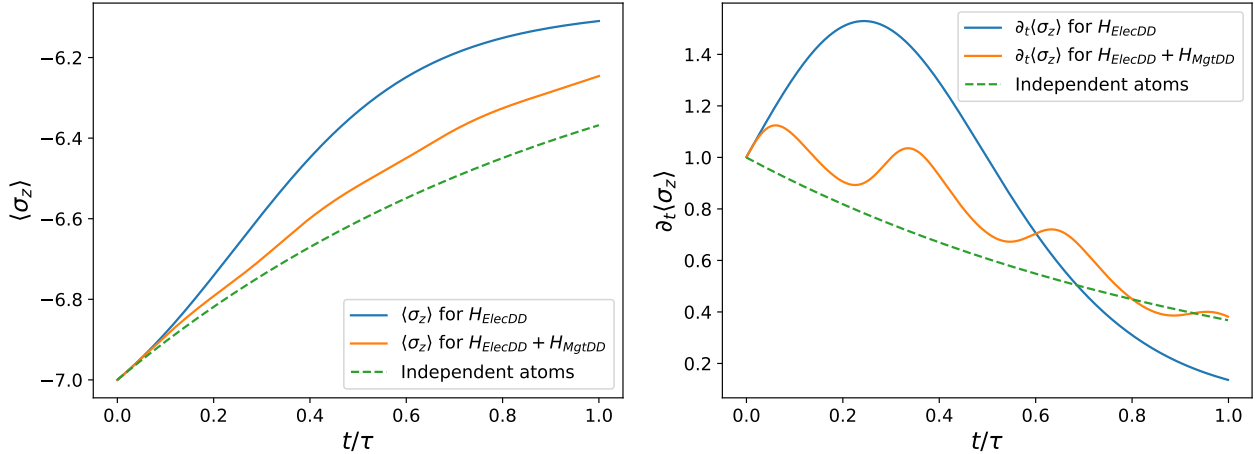


Figure 6: Time evolution of $\langle \sigma_z \rangle$ for a fully-inverted system in a lattice of $5 \times 5 \times 3 = 75$ atoms. Left: Time evolution of $\langle \sigma_z \rangle$. Right: Time derivates of $\langle \sigma_z \rangle$. The blue curve shows the evolution of a system where only the EDDI is taken into account, while the green dashed curved is for independent atoms (both are computed using the *CollectiveSpins.jl* library). The orange curve shows the evolution of the system when the EDDI, as well as the MDDI (through H_{MgtDD}) are also taken into account (using the symbolic derivation of the MPC equations method).

so the differential equations of the $\langle \sigma_i^z \rangle$ do not depend directly on this Hamiltonian. Indeed, we can write:

$$\partial_t \langle \sigma_i^z \rangle = \partial_t \text{Tr}(\rho \sigma_i^z) = \text{Tr}(\partial_t(\rho) \sigma_i^z) \quad (25)$$

And inserting the ME 1:

$$\partial_t \langle \sigma_i^z \rangle \propto \text{Tr}([H, \rho] \sigma_i^z) \propto \text{Tr}([H, \sigma_i^z] \rho) \quad (26)$$

using the cyclic properties of the trace. Finally, we know that $\text{Tr}([H_{MgtDD}, \sigma_i^z] \rho) = 0$ as H_{MgtDD} is only composed of products of σ_j^z operators. Thus for initial times, the $\langle \sigma_i^z \rangle$ will not depend on the presence or not of a MDDI.

However, the differential equations of $\langle \sigma_i^z \rangle$ also depend on 2-body correlations terms such as $\langle \sigma_i^{x/y} \sigma_j^{x/y} \rangle$. These correlations terms do not commute trivially with H_{MgtDD} because of the canonical commutation relationships of the Pauli operators. Thus we can reasonably think that the evolution of these correlations will be affected by the MDDI, and in return the expectation value $\langle \sigma_i^z \rangle$ also, but only after a certain amount of time.

- After this initial time, $\langle \sigma_z \rangle$ oscillates with a certain frequency. To try to understand the origin of these oscillations, let's take the simple case of 2 interacting atoms. We can analytically derive from the Schrödinger's equation the mean expectation value of the σ_x operator when both atoms start from the $|+x\rangle$ state, and are only interacting via H_{MgtDD} :

$$\langle \sigma_x \rangle = \frac{1}{2} \left(\cos \left(2 \frac{(a-b)}{\hbar} t \right) + \cos \left(2 \frac{(c-b)}{\hbar} t \right) \right) \quad (27)$$

We can see that the oscillations of $\langle \sigma_x \rangle$ depend on the difference of the $[a, b, c]$ frequencies of the MDDI. In figure 7, we plotted $\langle \sigma_x \rangle$ as a function of time, and the 2-body correlation function $\langle \sigma_1^x \sigma_2^x \rangle$, which oscillates at twice the frequency of $\langle \sigma_x \rangle$. Now if we look at the MPC equations given by our code⁶, we can see that the differential equation of $\langle \sigma_z \rangle$ depends on two-body correlations terms such as $\langle \sigma_1^x \sigma_2^x \rangle$, and it is thus reasonable to think that the oscillations visible in figure

⁶Refer to the GitHub repository or the theoretical description part of the documentation of the *CollectiveSpins.jl* library.

6 come from the 2-body correlation terms. We can finally add that the frequency of these oscillations and the ones of $\langle \sigma_1^x \sigma_2^x \rangle$ are likely to be different, as multiple correlation terms with different prefactors appear in the differential equations of $\langle \sigma_z \rangle$.

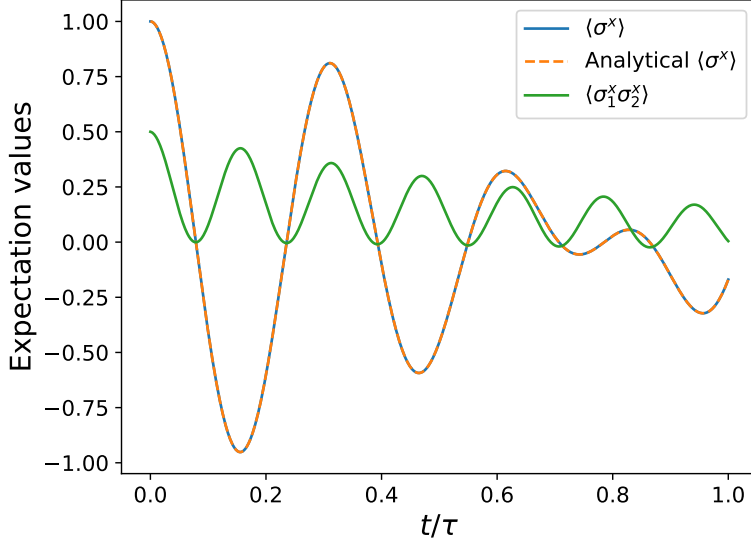


Figure 7: Oscillations of the expectation values of σ_x and of the 2-body correlation term $\langle \sigma_1^x \sigma_2^x \rangle$ as a function of time, for a $2 \times 1 \times 1$ lattice. The orange curve is the analytical derivation 27 of $\langle \sigma_x \rangle$, while the blue and green curves come from full quantum simulations of the Lindblad ME 1 with the *QuantumOptics.jl* library.

3 Exploring the experimental parameters

Until now, we simulated an ideal system and compared the decay of N atoms on a lattice interacting via the EDDI and MDDI. To bring the simulations closer to experimental reality, in this section, we will take into account a more detailed description of the excitation of the atoms (coherent *versus* incoherent excitations), the filling fraction of the lattice and harmonic trap detuning. We will also explore the dynamics of partial excitations of the system.

3.1 Coherent *versus* incoherent excitations

As already discussed in section 1.1, correlations and SR are deeply connected. When we start from an incoherent state (no correlations), for example from a fully-inverted system, the SR burst is only achieved after $t/\tau \approx 0.3$, because correlations need to be built up initially (see figure 4).

However, for a 2-level atom, the state can be described on the Bloch's sphere as:

$$|\Psi\rangle = \cos(\theta/2) |\downarrow\rangle + \sin(\theta/2) e^{i\varphi} |\uparrow\rangle \quad (28)$$

where θ and φ are the polar and azimuthal angles.

As the atoms are separated in space, the phase φ imposed by the laser during the excitation phase varies from one atom to the other. These phase differences create correlations between the atoms before they even start to interact, and can enhance SR⁷.

⁷The efficiency of the collective decay between 2 atoms depends on their phase, which is set by the laser during the excitation process, or by the virtual photons when atoms interact. To interact constructively and have the higher decay rate, the difference of phase of the two atoms must be equal to the one acquired by the virtual photon during its travel between the two atoms, which is exactly $\varphi = 2\pi \frac{d}{\lambda}$.

To add the laser induced phase, we consider a plane wave laser beam arriving in the horizontal plane of the lattice with an angle θ_l (see figure 3). In our experiment, $\theta_l \approx 30^\circ$. The following simulations use this value for the laser angle.

The phase φ for each atom is then simply $\varphi_i = 2\pi d_i/\lambda$ where d_i is the projection of the atom position vector \vec{r}_i (with respect to the first atom of the lattice⁸) on the laser beam vector (in red in figure 3).

To give an example of the importance of the coherence of the initial state on SR, we start from atoms in the equatorial plane of the Bloch's sphere ($\theta = \pi/2$), with atoms interacting only *via* the EDDI. We will call $|+x, \text{no corr}\rangle$ the initial state where all the atoms are in the $|+x\rangle$ state, and $|+x, \text{corr}\rangle$ the initial state where the azimuthal angle φ_i is set to $2\pi \frac{d_i}{\lambda}$ for each atom, which are still initially in the equatorial plane of the Bloch's sphere. We can see on figure 8 that the SR burst occurs from the beginning for the initial state $|+x, \text{corr}\rangle$, as the correlations are already built. Moreover, the maximum decay rate has much higher values than in the case with no laser induced correlations.

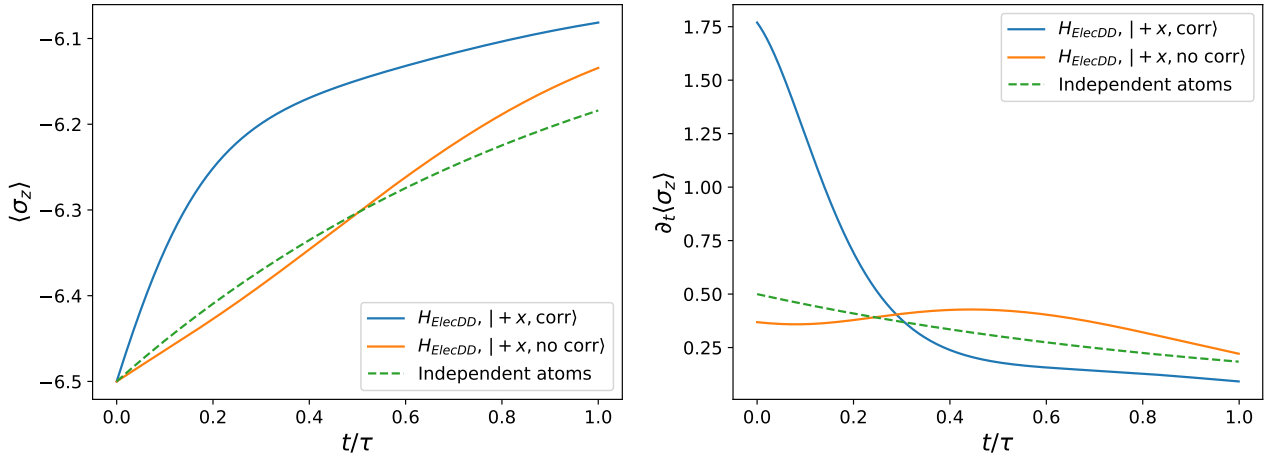


Figure 8: $\langle \sigma_z \rangle$ and its time derivative for a $5 \times 5 \times 3$ lattice with (blue curve) and without (orange curve) laser-induced correlations. Atoms interact only *via* the EDDI.

The MDDI is added on figure 9, starting from the $|+x, \text{corr}\rangle$ state. The initial decay rate is the same as when only the EDDI is taken into account, as discussed in section 2.3. However, it quickly drops down to low values, making SR difficult to characterise experimentally, even if we start from the $|+x, \text{corr}\rangle$ state.

Finally, we also scanned the SR criterium \mathcal{C} as a function of the angle θ_l to see the influence of the laser angle on SR (see figure 10). We can see that SR is enhanced for an angle of $\theta_l \approx 0.4 \text{ rad}$ and $\theta_l \approx 1.2 \text{ rad}$, and otherwise decreased. Moreover, the experimental situation is pretty close to the maximum achievable, which is reassuring. Finally, we can see on this plot that the SR criterium \mathcal{C} cannot distinguish between EDDI and EDDI + MDDI, as discussed in section 2.3, as the dynamics for these two cases are the same for initial times⁹.

⁸The specific atom used as the origin does not matter, as changing it only adds a global phase to all the atoms of the lattice.

⁹Moreover, as we wanted to see the influence of the laser angle, and thus the laser-induced correlations, on the decay of the system, we had to start from the $|+x, \text{corr}\rangle$, as the fully-inverted system cannot have these initial correlations. Thus the SR criterium \mathcal{C}_{\max} defined in the following section 3.2 will also not be able to distinguish between the 2 cases, as the SR burst occurs at $t = 0$ for this initial state. To see differences between the two cases on this plot, we should start from another initial state.

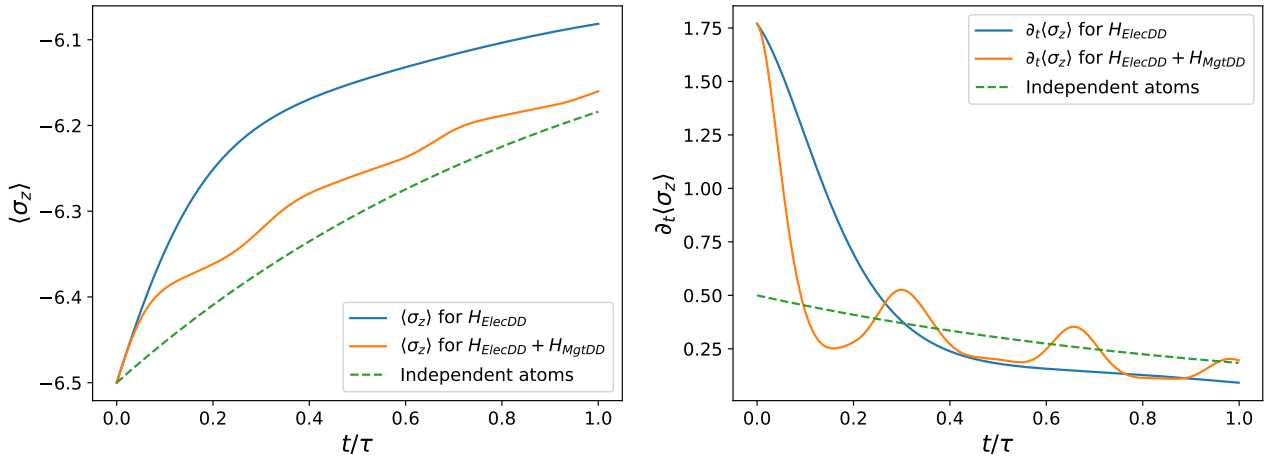


Figure 9: Starting from all the atoms in the $|+x, \text{corr}\rangle$. The lattice is $5 \times 5 \times 3$. We can see that the maximum decay rate is higher than in the fully-inverted case (see figure 6).

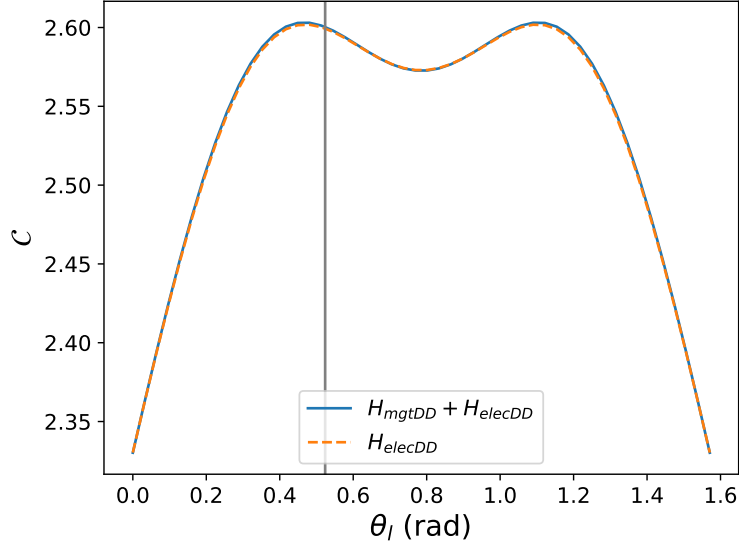


Figure 10: SR criterium C as a function of the angle of the laser beam θ_l , for an initial state $|+x, \text{corr}\rangle$. The lattice is $5 \times 5 \times 1$ atoms. In blue, we only have the electric interactions. In orange, we added H_{MgtDD} . The difference between the two is very small, as the SR criterium is computed at the initial time (see the discussion about this topic in section 2.3), but as we started for an initial $|+x, \text{corr}\rangle$ state to implement laser-induced correlations, the other SR criterium C_{max} would give similar results, as the SR burst occurs for initial times in this situation. The vertical grey line is the situation of the experiment, which is near the maximum achievable.

3.2 Initial number of ES

We will now explore the dynamics of a system where only N_{ES} atoms start from the ES, the other $N - N_{ES}$ being prepared in the GS¹⁰.

We randomly chose the N_{ES} atoms to initially set in the ES. As atoms are either in the GS or ES, we do not add any laser-induced phase φ . The distribution of excited atoms is random, so in order to get a general result independent of the specific distribution, we average the results over 10 different distributions (see figure 11). As we want to distinguish between the EDDI and EDDI + MDDI, our previous SR criterium is not sufficient, as we showed in section 2.3 that the initial dynamics are the same in both cases. We thus define a new criterium:

$$\mathcal{C}_{max} = \frac{\text{Max}(\partial_t \langle \sigma_z^z \rangle)}{\partial_t \langle \sigma_{idp}^z \rangle (t=0)} \quad (29)$$

which is the maximum decay rate of the system during the full dynamics normalised by the initial decay rate of the independent case. This criterium only works when we start from a fully-inverted system. Indeed, if we start from the $|+x, \text{corr}\rangle$ state, the SR burst happens at $t = 0$, and this criterium is equivalent to the first one \mathcal{C} .

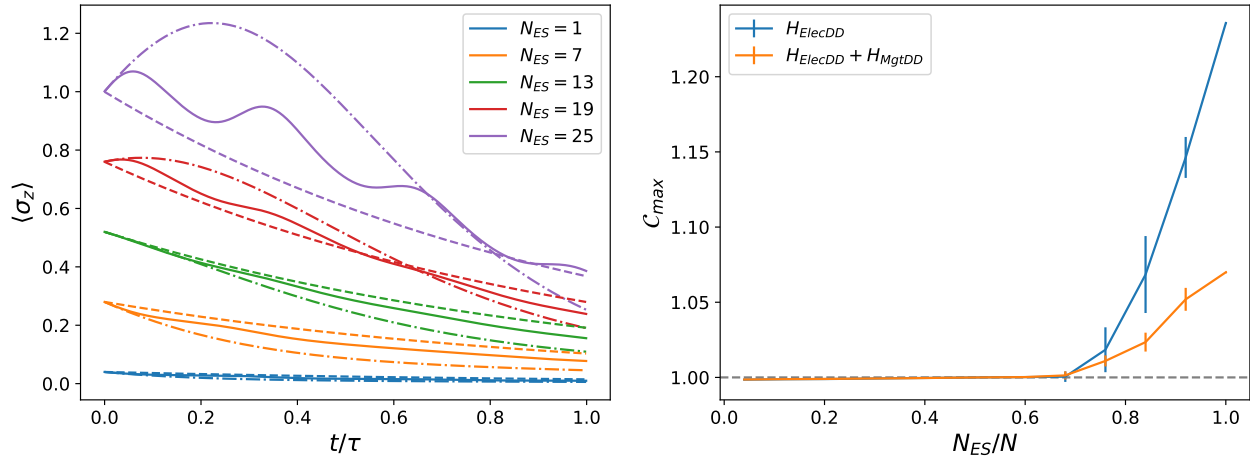


Figure 11: Left: Time derivative of $\langle \sigma_z^z \rangle$ as a function of time for varying number of initial ES N_{ES} (here, the results are plotted for single distributions). Solid lines: EDDI + MDDI. Dashed-dotted lines: EDDI only. Dotted lines: Independent case. The simulations are MPC computations realised for $5 \times 5 \times 1$ lattice. Right: SR criterium \mathcal{C}_{max} as a function of the number of initial ES. As the initial ES are chosen randomly on the N sites of the lattice, the MPC computations are averaged over 10 different distributions. The error bars are computed statistically from these distributions.

Under a certain number of initial ES (for $N = 13$ for instance), we can see on figure 11 that $\mathcal{C}_{max} < 1$, meaning that the system is Subradiant during the full dynamics (it will take more time to relax than the independent case). Indeed, as the atoms from the ES decay, they can also interact with atoms in the GS, and this interaction will slow down the total system decay.

3.3 Filling fraction

In the experiment, some lattice sites can be empty if no atoms were trapped during the preparation stage of the lattice. We define the filling fraction as: $\text{FF} = n/N$ where n is the number of occupied sites, and N the total number of sites of the lattice. Changing the filling fraction of the lattice is

¹⁰Actually this situation would be experimentally hard to achieve. Indeed, to prepare the atoms in the ES, we excite the system and then blow away the GS to keep only the atoms in the ES [Claude et al., 2024]. A maximum filling fraction of 97% can be achieved this way. See the following section 3.3 for a discussion on the filling fraction.

different than what we did in the previous section, when we changed the number of initial ES, as atoms in the GS were in this last situation still able to interact with the excited atoms (see section 3.2).

Simulations of varying FF were performed with a varying number n of randomly distributed atoms over a lattice of N sites (see figure 12). We plotted the SR criterium \mathcal{C}_{max} , starting from a fully-inverted system for the remaining atoms (as discussed previously, if we use \mathcal{C} or if we start from $|+x, \text{corr}\rangle$ we cannot distinguish between EDDI and EDDI + MDDI).

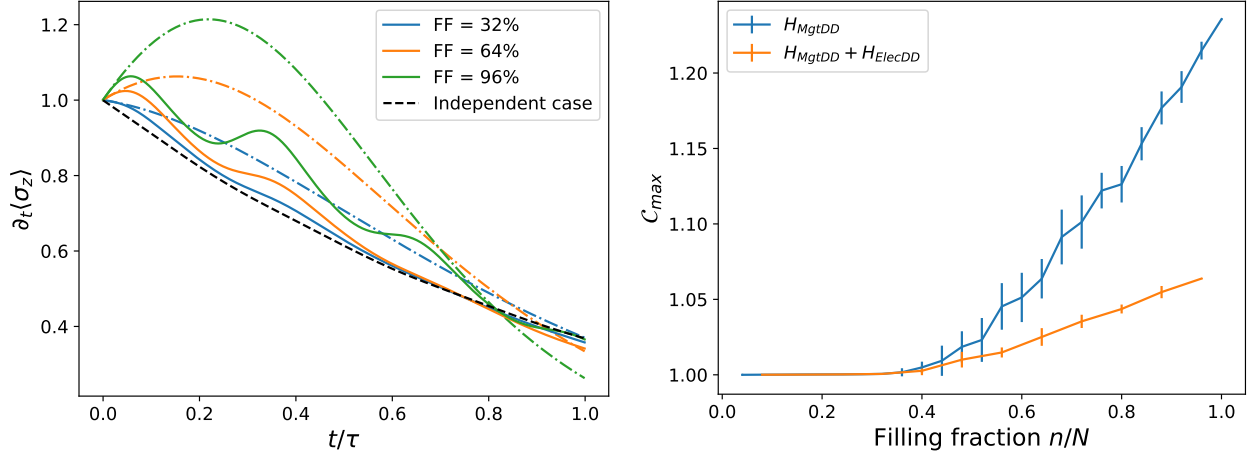


Figure 12: Simulations of varying FF were performed with n randomly distributed atoms over a lattice of $N = 5 \times 5 \times 1 = 25$ sites, for 10 different distributions, starting from all the atoms in the ES. Left: time-evolution of the derivatives $\partial_t \langle \sigma_z \rangle$. Solid lines: MDDI + EDDI. Dot-dashed lines: EDDI. Dashed black line: Independent case. Compared to 11, all the derivatives start from 1 as no atoms are in the GS at $t = 0$ (the expectation values are averaged on all the atoms remaining on the lattice). Right: SR criterium \mathcal{C}_{max} as a function of the FF. The blue curve is for H_{ElecDD} only, the orange one also takes into account H_{MgtDD} . \mathcal{C}_{max} doesn't scale as n^2 , as expected from section 1, because the distance between the atoms is effectively higher for low FF.

3.4 Harmonic trap detuning

A final experimental aspect that was taken into account in the simulations was the fact that atoms in the optical lattice do not experience the same trapping potential. Indeed, because the laser beams which create the lattice have a Gaussian profile, the trapping energies are higher at the center of the lattice than at its borders. The corresponding trapping energies will be approximated by a harmonic potential. Moreover, the atoms in the GS and ES also feel different trapping energies since they have different polarizabilities. Thus the trapping energy released when decaying from the ES to the GS is slightly different when comparing two different lattice sites. As only differences in energy matter, we can simulate this effect by adding to each atom a trapping energy to the ES proportional to d^2 , where d is the distance of the atom from the center of the lattice, and set the GS trapping energy to 0. The corresponding energy curves are plotted in the left plot of figure 13. The effect of this harmonic trap will thus be a detuning of the transition energy for each atom, which we would expect to lead to a decrease of the buildup of correlations.

To take the harmonic trap into account, we thus add to the EDDI and MDDI terms the following Hamiltonian (written in the single atom $\{| \uparrow \rangle, | \downarrow \rangle\}$ base) in our symbolic calculations:

$$H_{HT} = \begin{pmatrix} \omega_{HT}(d_i) & 0 \\ 0 & 0 \end{pmatrix} \quad (30)$$

where $\omega_{HT}(d_i) = \omega_{HT}^0 d_i^2$ and d_i is the distance of the considered atom from the centre of the lattice in units of lattice sites. In our experiment, we have: $\omega_{HT}^0 = 300 \text{ mHz/site}^2$.

In the right plot of figure 13, we plotted the evolution of the time derivative of $\langle \sigma_z \rangle$ with and without this additional Hamiltonian. We can see that the effect of the HT on the averaged spin values along the z-axis is relatively small, and slightly increases the oscillation frequency. Moreover, atoms with the same surroundings will not have the same dynamics. On figure 14, we showed the expectation values of σ_z for individual atoms. The red and orange curve for instance share the exact same surroundings (one at position $[0, 1, 0]$, the other at position $[0, 3, 0]$), but do not have the same dynamics, even though the atoms are at the same distance from the center of the lattice. The symmetry of the lattice is indeed broken by the laser beam. Indeed, we plotted the same curve, but with $\theta_l = 0$ in the appendix 3.4, and we see that these differences between equivalent lattice sites vanish.

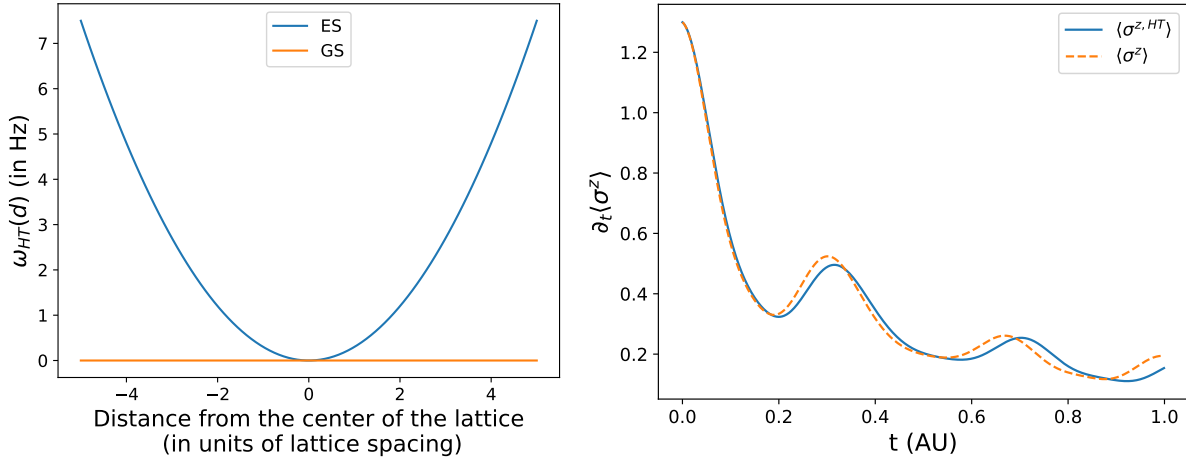


Figure 13: Left: ES and GS energies corresponding to the H_{HT} Hamiltonian, as a function of the distance from the center of the lattice. Right: Time derivatives of the expectation values of σ_z averaged over all the atoms for a $5 \times 5 \times 1$ lattice, with (blue) and without (orange) the detuning of the energies of the harmonic trap. Atoms start from the $|+x, \text{corr}\rangle$ state.

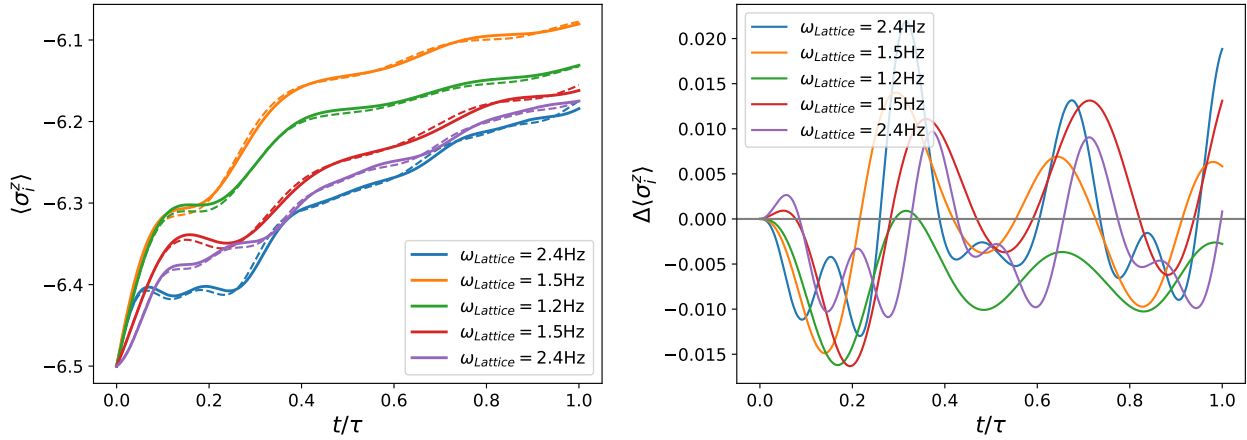


Figure 14: Left: Expectation value of σ_i^z for 5 atoms (located along a border of the lattice: the first one will have the position $[0, 0, 0]$, the second $[0, 1, 0]$ etc... until $[0, 4, 0]$). The legend gives there corresponding frequency $\omega_{HT}(d)$, in Hz. Dashed line: without H_{HT} . Right: Difference of $\langle \sigma_i^z \rangle$ with and without H_{HT} : $\Delta \langle \sigma_i^z \rangle = \langle \sigma_i^{z, HT} \rangle - \langle \sigma_i^z \rangle$.

Conclusion

The simulation of N interacting atoms is a complex problem, as the density matrix of the system scales exponentially with N. However, MPC simulations can be performed for a relatively high number of atoms, and they give a good approximation of the underlying dynamics of the system. To be able to add Hamiltonians at will, we used symbolic calculations to obtain the MPC equations. The resulting set of differential equations was then converted in C functions to be compiled in parallel, and solved in *Julia*. This method showed us that the magnetic interactions inherent to our reduced 2-level system of Erbium atoms tend to reduce the SR effect. Experimental details were finally explored, such as the coherence of the initial state, the filling fraction of the lattice or the harmonic trap detuning of the atoms, in order to characterise their impact on the collective decay of the atoms.

Preliminary data from the experiment did not show clear signs of SR, which might be attributed to the magnetic interactions in the system. In the future, one could try to tilt the magnetic field axis, as for a certain "magic" angle one can completely cancel the magnetic interactions in the horizontal plane.

Appendices

Table of symbols

Symbol	Signification
ES	Excited state
GS	Ground state
SR	Superradiance
SE	Spontaneous emission
γ	SE decay rate
τ	SE lifetime, $\tau = 1/\gamma$
$\sigma_i^{+/-}$	Single atom ladder operator
$\sigma^{+/-}$	Collective ladder operator (sum of the $\sigma_i^{+/-}$ over all the atoms)
EDDI	Electric dipole-dipole interaction (H_{ElecDD} + collective decay matrix Γ)
MDDI	Magnetic dipole-dipole interaction (H_{MgtDD})
MF	Meanfield
MPC	Meanfield plus correlations
λ	Wavelength of the laser
N_λ	Number of atoms which inter-distances is smaller than λ
$\langle \sigma^a \rangle$	Expectation value of the spin along the a -axis, averaged over all the atoms
$\langle \sigma_i^a \rangle$	Expectation value of the spin along the a -axis for the atom i
$d_{\downarrow\uparrow}$	Transition electric dipole moment
C	SR criterium of the initial decay rate
C_{max}	SR criterium of the maximum decay rate
μ_B	Bohr magneton
$\mu_{\uparrow\downarrow}$	Transition magnetic dipole moment
$\vec{\mu}_\uparrow$	Static magnetic dipole moment of the ES
$\vec{\mu}_\downarrow$	Static magnetic dipole moment of the GS
g_J	Landé g-factor for a total angular momentum J
μ_0	Vacuum magnetic permeability
e	Elementary charge
$ +x, \text{no corr}\rangle$	Initial state where all the atoms are in the $ +x\rangle$ state
$ +x, \text{corr}\rangle$	Initial state with $\theta = \pi/2$ and laser-induced φ_i in the Bloch's sphere representation
HT	Harmonic trap

Experimental side-projects

EOM

In order to stabilise the frequency of one of the lasers used in the experiment, we had to lock its frequency, thanks to a cavity. Moreover, as we wanted the locked frequency to be tunable, we needed to test an electro-optic modulator (EOM) that will be added to the preparation stage of the laser beam (see figure 15). This was done using a *LNY8510A* phase modulator from *Thorlabs*, that can respond to frequencies up to 10 GHz.

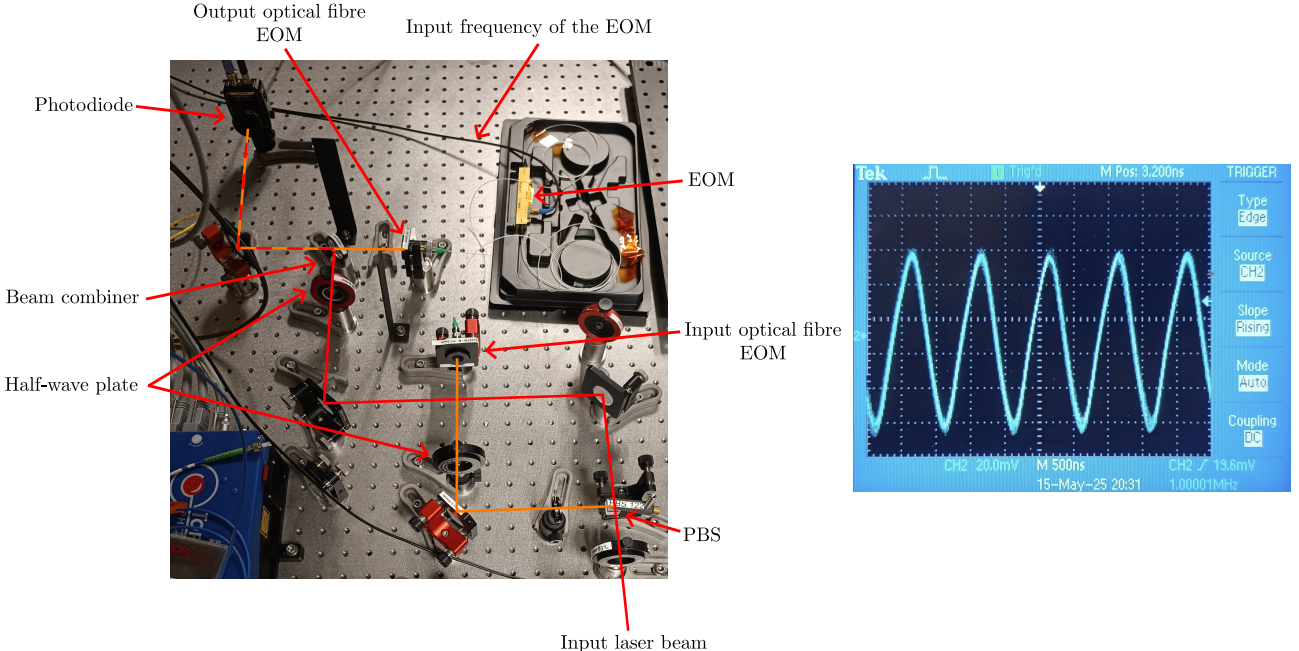


Figure 15: Left: optical setup of the EOM. The laser beam input is at the bottom of the picture. The beam is first separated in two beams thanks to a polarising beam-splitter (PBS). One beam will go through the EOM (orange) while the other (in red) is directly send to the photodiode. To get interferences, the two beams must share the same polarisation. To do so, we add a half-wave plate (at the left of the setup) to tune the polarisation of the beam that doesn't go through the EOM. Another half-wave plate is used at the center of the setup to optimise the coupling of the laser with the optic fibre and with the EOM. The EOM is supplied by a high-frequency electric signal (the corresponding cable is visible at the top of the setup). Finally, the two beams are recombined thanks to a beam combiner, before entering the photodiode. Right: Signal of the photodiode, read by an oscilloscope. The frequency set to the EOM is 1 MHz. The signals are not perfectly sinusoidal, as the laser and the EOM were not phase-locked.

Frame for the camera

The camera was held only by its objective, which created some vibrations, mostly because of the fan cooling the camera. These vibrations reduced the quality of the images. Indeed, to take a measurement, three different pictures are taken by the camera. The first one is with the atoms and the lasers on, the second with only the lasers and the final one is without any atoms or laser. The final image is created by subtracting these different pictures, to keep only the atoms. If some vibrations are present, the camera moves in between these pictures, and the final image is noisy. To reduce these vibrations, a support was modelled on *SolidWorks*, and 3D printed out (see figure 16).



Figure 16: The support of the camera is the black rectangle frame.

Digital PID

To control the power of a laser beam, a proportional integral derivative controller (PID) is used in the experiment. A PID controls a signal which has to be set to a certain value. An error is calculated from the difference between the real value of the signal and the target signal. A correction with three components is then applied to reduce this error. The first is a proportional correction to provide immediate corrections, the second is an integral component to remove steady-state residuals and the final one is a derivative component to increase the stability of the response.

In the experiment, a small part of the laser beam is redirected to a photodiode to measure the beam power. The PID is then performed, and the correction is applied to the beam with an EOM. The PID used is analogue, and is rather complicated to manipulate. As analogue-to-digital converter (ADC) and digital-to-analogue converter (DAC) chips can achieve very high frequencies and accuracy, and are relatively cheap, the idea was to see how good a fully digital PID could be compared to the analogue one (see figure 17).

For the ADC, we used the *AD4000* from *Analogue Devices*. It is a 16-bit chip that can convert analogue signals up to 2.10^6 signals/s. For the DAC, we used the *AD5689R* from the same company, which can convert a digital signal to an analogue one with 16-bit accuracy and up to a few MHz. Finally, to compute the PID, we plugged these two components to a *Teensy4.1*, which is a microcontroller that can run up to 1 GHz.

However, this project was not implemented to the experiment due to a lack of time. As my internship will continue until mid-July, I hope to finish this project!

Derivation of the Master Equation

A step-by-step derivation of the Lindblad master equation can be found in [Manzano, 2020] and [Carmichael, 2009]. We will describe a little bit more precisely in this appendix the approximations needed to get the ME.

- Born approximation: the interaction between the system and the environment are approximated to second order.
- Markov approximation: The environment is large enough so that the time scale of its dynamics is much bigger than the time scale of the system. This approximation transforms the differential equation of the density matrix into a Markovian system (the future behaviour of the system depends only on its present state, and not on its past states).
- At $t = 0$, we assume that no correlations exist between the system and the environment.

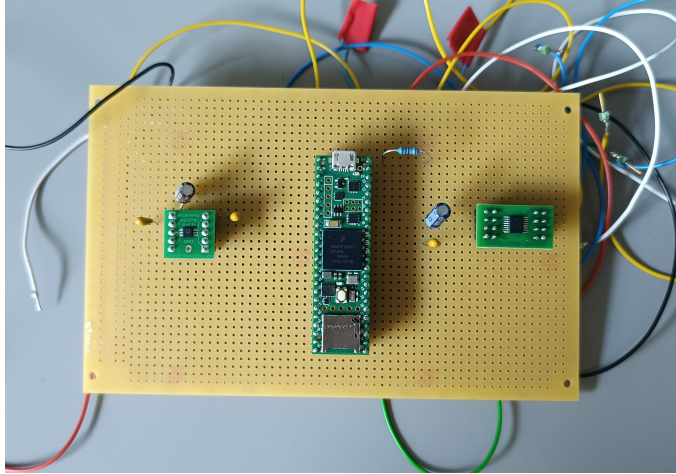


Figure 17: The digital PID breadboard. The ADC is on the right, and the DAC on the left. The *Teensy4.1* microcontroller is at the center.

- Rotating-wave approximation: terms oscillating much faster than the other ones can be averaged to zero, and thus neglected. See section 3.4 for a discussion on this approximation.

As all these approximations are valid in the context of our experiment, we can use the Lindblad master equation to model our system.

Cumulant expansion

When deriving the MF/MPC equations (see 1.3), the differential equations of the correlation functions of order n will depend on correlation terms of order $n + 1$. To close the set of differential equations at the order n , we thus need to approximate correlations functions of order $n + 1$ and write them as a product of terms of order $\leq n$. We do this thanks to a cumulant expansion method [Kubo, 1962].

The joint cumulant of n operators can be written as:

$$\langle X_1 X_2 \dots X_n \rangle_c = \sum_{p \in P(I)} (|p| - 1)! (-1)^{|p|-1} \prod_{B \in p} \langle \prod_{i \in B} X_i \rangle \quad (31)$$

The joint cumulant can be thought of as a measurement of the correlation between operators. Thus, if we assume that the joint cumulant of order n is zero, we can write $\langle X_1 X_2 \dots X_n \rangle$ as a function of correlation functions of order $\leq n - 1$.

Solving algorithm

The solver algorithm used in the codes is the Dormand-Prince method [Dormand and Prince, 1980]. Let's make a brief recap on the Runge-Kutta method:

For a differential equation :

$$\partial_t y(t) = f(t, y) \text{ and } y(t_0) = y_0 \quad (32)$$

the Runge-Kutta (RK) method gives the following estimation:

$$y_{n+1} = y_n + h \sum_{i=1}^s b_i k_i \quad (33)$$

where y_{n+1} is the RK approximation of $y(t_{n+1}) = y(t_n + h)$ and s is the number of stage.

The function evaluations k_i are defined as

$$k_i = f(t_n + c_i h, y_n + (a_{i,1} k_1 + a_{i,2} k_2 + \dots + a_{i,i-1} k_{i-1}) h) \quad (34)$$

where $c_1 = 0$, $a_{i,j}$, b_i and c_i are the coefficients of the method, and h is the time step. The k_i will thus be the derivatives of the function $y(t)$ for several points between y_n and y_{n+1} (the coefficients values are between 0 and 1).

The Dormand-Prince method uses six function evaluations to calculate fourth and fifth order accurate solutions (where the order m of a solution means that the total accumulated error is in $\mathcal{O}(h^m)$). The difference between these two accurate solutions gives an estimation of the error of the fourth order, which is used to optimise the time step.

Comparison of the computation time

In the following array, a few computation time and the corresponding memory allocated during the simulation for the full solution of the ME are given. We can see that above 8 atoms, the simulation slows down a lot and the memory used diverges, restraining this method. As a comparison, the MPC simulations for a $5 \times 5 \times 3$ lattice with MDDI and EDDI takes 511.3 s with 569.6 MB allocated. For a $5 \times 5 \times 1$ lattice this time is reduced to 15.5 s with 376.2 MB allocated.

Nbr of atoms	Full Quantum solution
2	5 s, 1004 MB
4	5 s, 1009 MB
8	103 s, 2 GB
10	2071 s, 17 GB

Derivation of the H_{MgtDD} used in the simulations

If we keep the operators of a Spin(1/2) system and then map the spin values to $[-7, -6]$, we will not properly simulate our system. Let's take a 2 atoms example to illustrate this:

- For a 2 atoms Spin(1/2) system, $\sigma_z = \begin{pmatrix} 1 & 0 \\ 0 & -1 \end{pmatrix}$. Thus, the states $|\uparrow\downarrow\rangle$ and $|\downarrow\uparrow\rangle$ will have a negative energy, while the states $|\uparrow\uparrow\rangle$ and $|\downarrow\downarrow\rangle$ will have a positive energy, leading to a preferred antiferromagnetic configuration.
- For a -6/-7 system, $\sigma_z = \begin{pmatrix} -7 & 0 \\ 0 & -6 \end{pmatrix}$ and the favored configuration is $|\downarrow\downarrow\rangle$.

Instead of working with the Pauli matrices, we will thus work with the population operators in the ES and GS in order to remove this issue concerning the sign of the different spin states (see equation 23). Finally, we will approximate this interaction as a nearest-neighbours interaction, as the effects of the dipole interaction scale as $1/r^3$ with r the distance between two atoms (see equation 21).

Role of the dimension and MPC error

In this subsection, we will explore the role of the dimension of the lattice in the decay of a system of N atoms interacting via the EDDI only for a N 2-level system with energies $-1/+1$ for the GS/ES. We will also compare full quantum, MF and MPC simulations.

MPC error and role of the dimensionality of the lattice for the EDDI

We can see from figure 18 that only the MPC and the full computation of the ME correctly predict the SR decay. MF, as it doesn't take into account 2-body correlations between the atoms, cannot predict the collective decay behaviour, and just show the classical SE decay, also exhibited by independent atoms.

The error of the MPC approach compared to the full quantum computation is relatively small, at least for normalised simulation times smaller than one ($t/\tau \leq 1$), regardless of the dimensions of the lattice.

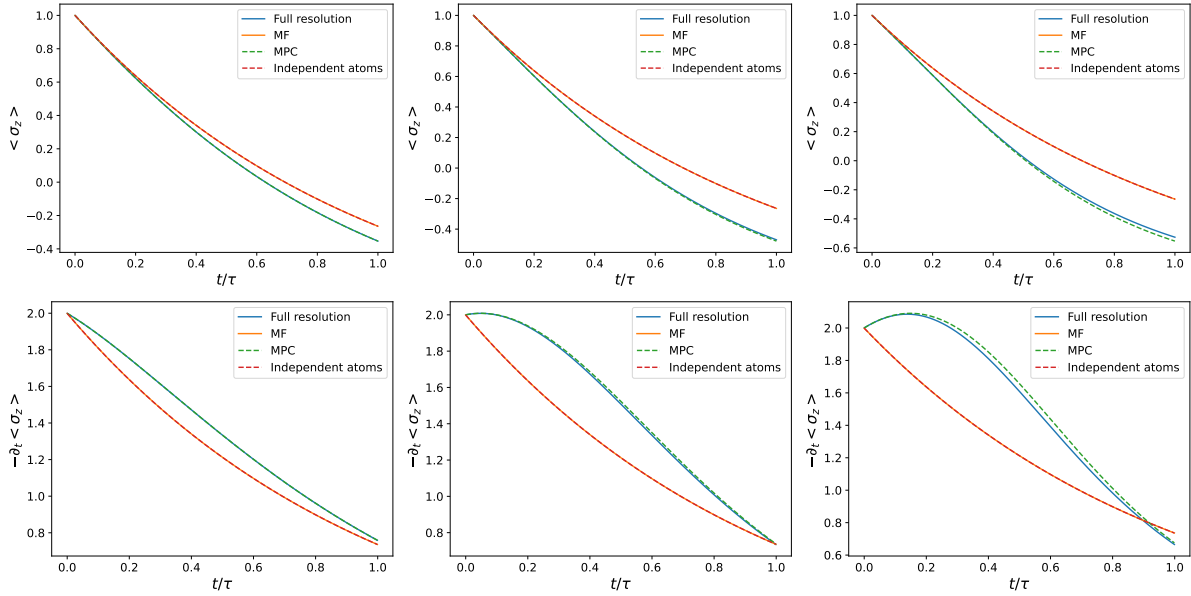


Figure 18: Role of the dimensionality and comparison between a full computation of the ME, MF and MPC computations. The mean average expectation value $\langle \sigma_z \rangle$ (top figures) and its corresponding decay rate (bottom figures) is plotted with respect to time, for different lattices. A minus sign is added for the decay rate, as the spin of the atom decreases from 1 to -1 during the decay. Left: $2 \times 1 \times 1$ lattice. Center: $2 \times 2 \times 1$ lattice. Right: $2 \times 2 \times 2$ lattice. At $t = 0$, all the atoms are in the ES (fully-inverted system). To get the real values of $\langle \sigma_z \rangle$, one only has to map from $[-1, +1] \rightarrow [-6, -7]$ (see the discussion on this matter at section 2).

Comparison between full Quantum computation and MPC for the EDDI + MDDI

In this subsection, we will compare the simulations results of the symbolic derivation of the MPC equations method with respect to the full computation of the Lindblad ME for the EDDI + MDDI case. We can on figure 19 see oscillations of $\langle \sigma_z \rangle$ even in the full quantum case, meaning that these oscillations do not come from the fact that we stopped at the second order in the MPC simulations. For relatively small times, we can see that the error of the MPC approach remains small.

Influence of θ_l for the individual dynamics of the atoms with EDDI + MDDI in a harmonic trap

We saw in figure 14 that atoms in position $[0, 2, 0]$ and $[0, 4, 0]$ do not have the same dynamics in a lattice of $5 \times 5 \times 1$. This is concerning, as they share the exact same surroundings configurations and distance from the center of the lattice. However, the laser-induced phase will not be the same for the two atoms and their neighbours. If we set $\theta_l = 0$, we can see that the dynamics for symmetric atoms are the same (see figure 20).

Rabi oscillations

In this section, we will describe a little bit more precisely the Rabi oscillations, which appear when atoms interact with a laser beam.

Rotating-wave approximation

Let's consider a single 2-level atom. The atomic corresponding Hamiltonian can be written as:

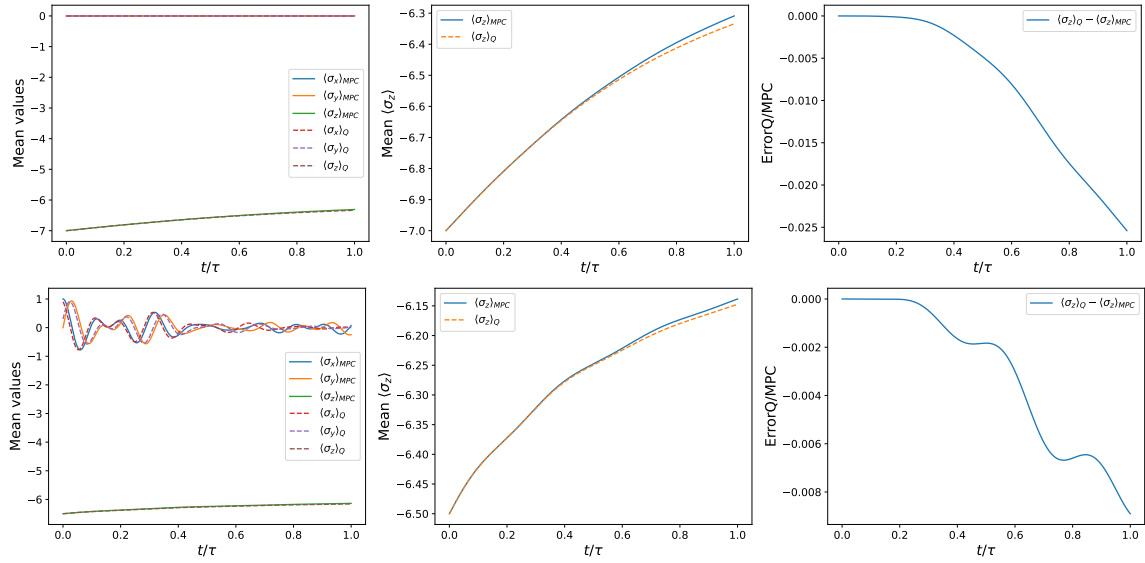


Figure 19: Comparison between a full computation of the ME and a MPC simulation for EDDI + MDDI in a lattice of $1 \times 2 \times 4$ atoms. Up: Fully inverted system. Bottom: Starting from the $|+x, \text{corr}\rangle$ state. Left: Mean $\langle \sigma_{x/y/z} \rangle$ evolution as a function of time. In the legend, Q stands for full ME computation, and MPC for meanfield plus correlations. Middle: Evolution of the mean $\langle \sigma_z \rangle$ only. Right: Difference between full computation of the ME and MPC simulations for the mean $\langle \sigma_z \rangle$ expectation value averaged over all the atoms. We can see that the results of the MPC approach are relatively accurate as long as $t/\tau \leq 1$.

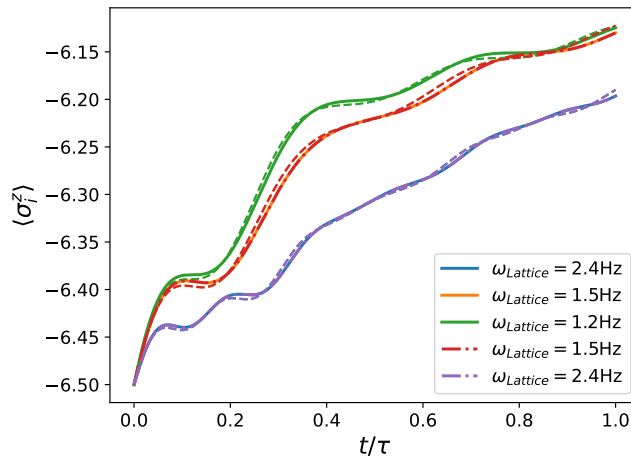


Figure 20: If we set $\theta_l = 0$, we can see that atoms in symmetric position in the lattice will have the same dynamics. This explains why atoms didn't share the same dynamics in figure 14.

$$H_0 = \frac{\hbar\omega_0}{2}\sigma_z \quad (35)$$

where ω_0 is the atomic frequency of the transition between the GS and the ES.

Now let's add a slightly detuned laser beam, whose electric field can be written as:

$$\vec{E}(t) = \vec{E}_0 e^{-i\omega_L t} + \vec{E}_0^* e^{i\omega_L t} \quad (36)$$

where \vec{E}_0 is the amplitude of the electromagnetic field, and ω_L its frequency.

The Hamiltonian of the interaction between the atom and the laser can then be written as:

$$H_1 = -\mathbf{d} \cdot \vec{E} \quad (37)$$

where \mathbf{d} is the electric transition dipole moment operator of the atom (define in equation 8).

If we develop H_1 in the interaction picture, we get:

$$H_{1,I} = -\hbar \left(\Omega e^{-i\Delta\omega t} + \tilde{\Omega} e^{i(\omega_L + \omega_0)t} \right) \sigma^+ - \hbar \left(\tilde{\Omega}^* e^{-i(\omega_L + \omega_0)t} + \Omega^* e^{i\Delta\omega t} \right) \sigma^- \quad (38)$$

where $\Omega = \vec{d}_{\downarrow\downarrow} \cdot \vec{E}_0 / \hbar$ is the Rabi frequency, $\tilde{\Omega} = \vec{d}_{\downarrow\downarrow} \cdot \vec{E}_0^* / \hbar$ is the counter-rotating frequency, and $\Delta\omega = \omega_l - \omega_0$ is the detuning of the laser.

The rotating-wave approximation that we made in the derivation of the ME (see section 3.4) consists in neglecting the rapidly oscillating terms, where the sum of the frequencies appear. A plot of the dynamics of $\langle \sigma_z \rangle$ for a single atom with and without the RWA can be seen in figure 21.

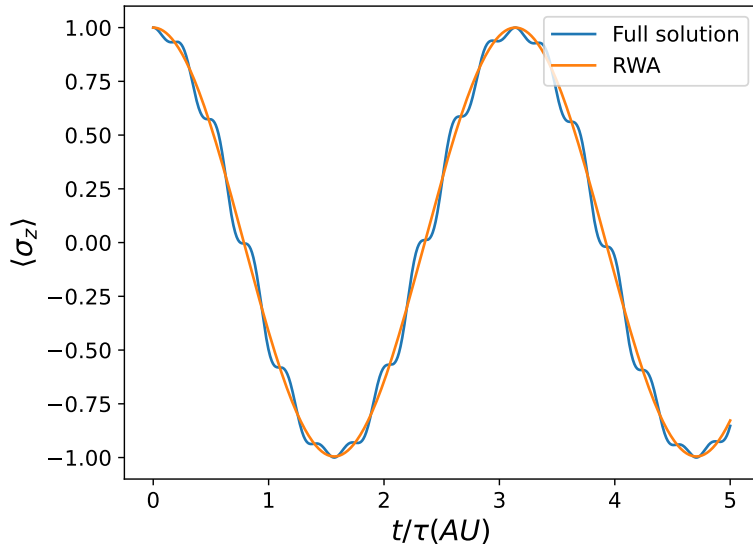


Figure 21: Evolution of $\langle \sigma_z \rangle$ as a function of time with and without the RWA. Here, the atomic frequency is $\omega_0 = 10$ Hz, and $\omega_l = 11$ Hz, so the relative detuning $(\omega_l - \omega_0)/\omega_0 = 10\%$. The smaller this relative detuning is, the better the approximation is. In the experiment, the typical values of the detuning are a few kHz while the order of magnitudes of the optical frequencies are hundreds of THz, so the RWA is completely valid in our case.

If we add the EDDI for a $2 \times 2 \times 2$ lattice (see figure 22), we can see that the RWA is still good, as it only removes the rapid oscillations of $\langle \sigma_z \rangle$, which completely vanish if we take the real values of the frequencies.

A concerning fact is that we know from the experiment that atoms cannot be excited by a laser if the detuning is too important. This upper-boundary of the detuning is very low (a few kHz in our case). This must not be confused with Rabi oscillations, as this effect is taken care of in the probability

coefficient of transition. For instance, if an atom is excited, the probability that his spin flips because of the driving laser is:

$$P_{\uparrow \rightarrow \downarrow} = \frac{\Omega^2}{\Omega_g^2} \sin^2 \left(\frac{\Omega_g}{2} t \right) \quad (39)$$

where $\Omega_g = \sqrt{\Delta\omega^2 + \Omega^2}$ is the generalised Rabi frequency. We can clearly see that if the detuning is too important compared to the Rabi frequency, the laser will not interact with the atom.

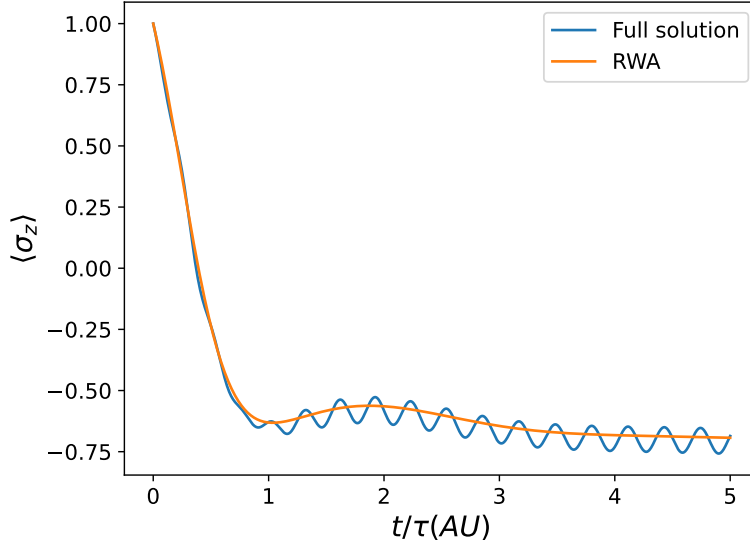


Figure 22: Comparison with and without the RWA for a $2 \times 2 \times 2$ lattice. The frequencies are the same as on figure 21. The rapid oscillations of the full solution completely vanish if we take the real relative detuning of our experiment.

Random detuning of the frequencies

In the experiment, the energy levels of our 2-level atoms can vary, because of external noises such as perturbation in the external magnetic/electric field. We wanted to take into account this phenomenon in the study of the Rabi oscillations. To do so, we implemented a toy model with EDDI only, for a lattice of dimensions $2 \times 2 \times 2$. The frequency are the same as the one used in section 3.4. Adding a random noise (a few Hz) to the energy of each ES (see left plot on figure 23) changes the Rabi oscillations. We can see on the right plot of figure 23 that the Rabi oscillations frequency is slightly decreased. More importantly, the oscillations quickly become incoherent (no longer a sin-wave) as the atoms oscillate with different frequencies.

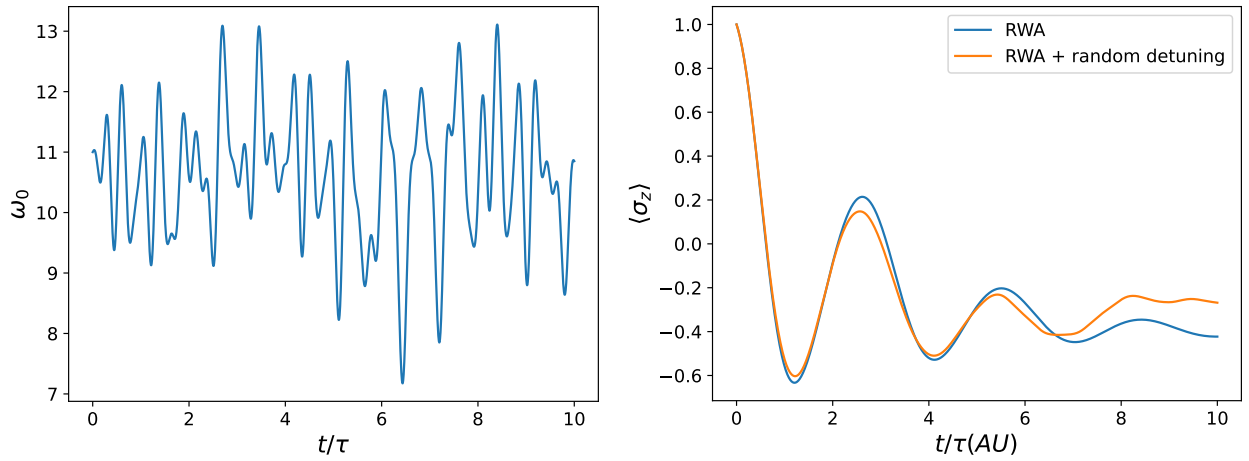


Figure 23: Left: Energy level of the ES of one atom of the lattice. Every atom has the same kind of random energy evolution of its ES. Right: Expectation values of $\langle \sigma_z \rangle$ with (orange curve) and without (blue curve) the random detuning of the ES for each atom.

References

- [Baßler et al., 2024] Baßler, N. S., Varma, I., Proske, M., Windpassinger, P., Schmidt, K., and Genes, C. (2024). Cooperative effects in dense cold atomic gases including magnetic dipole interactions. *Physical Review Research*, 6(2):023147.
- [Bettles et al., 2016] Bettles, R. J., Gardiner, S. A., and Adams, C. S. (2016). Cooperative eigenmodes and scattering in one-dimensional atomic arrays. *Physical Review A*, 94(4):043844.
- [Carmichael, 2009] Carmichael, H. (2009). *An open systems approach to quantum optics: lectures presented at the Université Libre de Bruxelles, October 28 to November 4, 1991*, volume 18. Springer Science & Business Media.
- [Chomaz et al., 2022] Chomaz, L., Ferrier-Barbut, I., Ferlaino, F., Laburthe-Tolra, B., Lev, B. L., and Pfau, T. (2022). Dipolar physics: a review of experiments with magnetic quantum gases. *Reports on Progress in Physics*, 86(2):026401.
- [Claude et al., 2024] Claude, F., Lafforgue, L., Houwman, J., Mark, M. J., and Ferlaino, F. (2024). Optical manipulation of spin states in ultracold magnetic atoms via an inner-shell hz transition. *Physical Review Research*, 6(4):L042016.
- [Dicke, 1954] Dicke, R. H. (1954). Coherence in spontaneous radiation processes. *Physical review*, 93(1):99.
- [Dormand and Prince, 1980] Dormand, J. R. and Prince, P. J. (1980). A family of embedded runge-kutta formulae. *Journal of computational and applied mathematics*, 6(1):19–26.
- [Gorshkov et al., 2011] Gorshkov, A. V., Manmana, S. R., Chen, G., Ye, J., Demler, E., Lukin, M. D., and Rey, A. M. (2011). Tunable superfluidity and quantum magnetism with ultracold polar molecules. *Physical review letters*, 107(11):115301.
- [Gross and Haroche, 1982] Gross, M. and Haroche, S. (1982). Superradiance: An essay on the theory of collective spontaneous emission. *Physics reports*, 93(5):301–396.
- [Inouye et al., 1999] Inouye, S., Chikkatur, A., Stamper-Kurn, D., Stenger, J., Pritchard, D., and Ketterle, W. (1999). Superradiant rayleigh scattering from a bose-einstein condensate. *Science*, 285(5427):571–574.
- [Jackson, 2021] Jackson, J. D. (2021). *Classical electrodynamics*. John Wiley & Sons.
- [Kubo, 1962] Kubo, R. (1962). Generalized cumulant expansion method. *Journal of the Physical Society of Japan*, 17(7):1100–1120.
- [Manzano, 2020] Manzano, D. (2020). A short introduction to the lindblad master equation. *Aip advances*, 10(2).
- [Masson et al., 2024] Masson, S. J., Covey, J. P., Will, S., and Asenjo-Garcia, A. (2024). Dicke superradiance in ordered arrays of multilevel atoms. *PRX Quantum*, 5(1):010344.
- [Natale, 2017] Natale, G. (2017). Spin physics in dipolar quantum gases of erbium atoms.
- [Plankensteiner et al., 2022] Plankensteiner, D., Hotter, C., and Ritsch, H. (2022). Quantumcumulants.jl: A julia framework for generalized mean-field equations in open quantum systems. *Quantum*, 6:617.
- [Poli et al., 2023] Poli, E., Bland, T., White, S. J., Mark, M. J., Ferlaino, F., Trabucco, S., and Mannarelli, M. (2023). Glitches in rotating supersolids. *Physical Review Letters*, 131(22):223401.

[Rackauckas and Nie, 2017] Rackauckas, C. and Nie, Q. (2017). DifferentialEquations.jl—a performant and feature-rich ecosystem for solving differential equations in Julia. *Journal of Open Research Software*, 5(1).

[Rui et al., 2020] Rui, J., Wei, D., Rubio-Abadal, A., Hollerith, S., Zeiher, J., Stamper-Kurn, D. M., Gross, C., and Bloch, I. (2020). A subradiant optical mirror formed by a single structured atomic layer. *Nature*, 583(7816):369–374.

[Smith and Spalding, 1961] Smith, K. and Spalding, I. (1961). The atomic g values of some rare-earth atoms. *Proceedings of the Royal Society of London. Series A. Mathematical and Physical Sciences*, 265(1320):133–140.